Comparison of drifting buoy velocities to HF radar radial velocities from the Ocean Networks Canada Strait of Georgia 25 MHz CODAR array

Mark Halverson, Jim Gower, Rich Pawlowicz

Fisheries and Oceans Canada
Institute of Ocean Sciences
9860 West Saanich Road
Sidney, British Columbia
V8L 4B2

2018

Canadian Technical Report of Hydrography and Ocean Sciences 319

Fisheries and Oceans Canada | Pêches et Océans Canada | Canada

Canadian Technical Report of Hydrography and Ocean Sciences

Technical reports contain scientific and technical information of a type that represents a contribution to existing knowledge but which is not normally found in the primary literature. The subject matter is generally related to programs and interests of the Oceans and Science sectors of Fisheries and Oceans Canada.

Technical reports may be cited as full publications. The correct citation appears above the abstract of each report. Each report is abstracted in the data base *Aquatic Sciences and Fisheries Abstracts.*

Technical reports are produced regionally but are numbered nationally. Requests for individual reports will be filled by the issuing establishment listed on the front cover and title page.

Regional and headquarters establishments of Ocean Science and Surveys ceased publication of their various report series as of December 1981. A complete listing of these publications and the last number issued under each title are published in the *Canadian Journal of Fisheries and Aquatic Sciences*, Volume 38: Index to Publications 1981. The current series began with Report Number 1 in January 1982.

Rapport technique canadien sur l'hydrographie et les sciences océaniques

Les rapports techniques contiennent des renseignements scientifiques et techniques qui constituent une contribution aux connaissances actuelles mais que l'on ne trouve pas normalement dans les revues scientifiques. Le sujet est généralement rattaché aux programmes et intérêts des secteurs des Océans et des Sciences de Pêches et Océans Canada.

Les rapports techniques peuvent être cités comme des publications à part entière. Le titre exact figure au-dessus du résumé de chaque rapport. Les rapports techniques sont résumés dans la base de données *Résumés des sciences aquatiques et halieutiques.*

Les rapports techniques sont produits à l'échelon régional, mais numérotés à l'échelon national. Les demandes de rapports seront satisfaites par l'établissement auteur dont le nom figure sur la couverture et la page de titre.

Les établissements de l'ancien secteur des Sciences et Levés océaniques dans les régions et à l'administration centrale ont cessé de publier leurs diverses séries de rapports en décembre 1981. Vous trouverez dans l'index des publications du volume 38 du *Journal canadien des sciences halieutiques et aquatiques*, la liste de ces publications ainsi que le dernier numéro paru dans chaque catégorie. La nouvelle série a commencé avec la publication du rapport numéro 1 en janvier 1982.

Canadian Technical Report of Hydrography and Ocean Sciences 319

2018

Comparison of drifting buoy velocities to HF radar radial velocities from the Ocean Networks Canada Strait of Georgia 25 MHz CODAR array

by

Mark Halverson[1], Jim Gower[2], Rich Pawlowicz[1]

Ocean Science
Department of Fisheries and Oceans
9860 West Saanich Road
Sidney, British Columbia
V8L 4B2

[1]Department of Earth, Ocean, and Atmospheric Sciences, University of British Columbia, Vancouver, BC, V6T 1Z4

[2]Ocean Science, Department of Fisheries and Oceans, 9860 West Saanich Road, Sidney, British Columbia V8L 4B2

Cat. No. Fs97-18/319E-PDF ISBN 978-0-660-23618-6 ISSN 1488-5417

Correct citation for this publication:

Halverson, M., Gower, J., and Pawlowicz, R. 2018. Comparison of drifting buoy velocities to HF radar radial velocities from the Ocean Networks Canada Strait of Georgia 25 MHz CODAR array. Can. Tech. Rep. Hydrogr. Ocean Sci. 319: vi + 38 p.

Contents

List of Figures

List of Tables

Abstract

Halverson, M., Gower, J., and Pawlowicz, R. 2018. Comparison of drifting buoy velocities to HF radar radial velocities from the Ocean Networks Canada Strait of Georgia 25 MHz CODAR array. Can. Tech. Rep. Hydrogr. Ocean Sci. 319: vi + 38 p.

Near-surface flow velocities were computed from a series of drifting buoy deployments in the Strait of Georgia, BC, Canada, and compared to radial velocities measured by two 25 MHz HF radar systems with the goal of characterizing the accuracy and precision of the radar measurements. Two drifter drogue styles were used, with effective sampling depths of 0.35 m and 1 m, allowing us to investigate which drifter more closely matches the radar velocities.

The radar/drifter velocity difference was quantified with the following statistics: bias, RMS difference, coefficient of determination (r^2), and linear regression. Measurement bias, $\langle V_r^{radar} - V_r^{drifter} \rangle$, ranged from 0 to -5 cm/s depending on the drifter/radar pair, indicating that the drifters measure a faster flow on average. RMS velocity differences ranged from 11.3 to 17.2 cm/s, which are relatively high in comparison to other CODAR systems. r^2 ranged from 0.46 to 0.81, reflecting the relatively high RMS error. Linear functions were fit to the radar/drifter regressions, and the slopes of the fitted lines indicate that the drifter velocities are about 20% and 30% higher than the HF radar measurements for the 1 m and 0.35 m drifters, respectively, and that the velocity difference increases with flow speed.

The shallow drogued drifters routinely measure higher velocities than the deeper drifters, and the deeper drifters measure higher velocities than the HF radar despite sampling deeper water. This could imply that the radar measures only the Eulerian part of the drift speed, however the results are only suggestive because of the relatively high statistical uncertainty in the drifter/radar comparison and the potential for the HF radar velocities to be biased low at high flow speeds.

Résumé

Halverson, M., Gower, J., and Pawlowicz, R. 2018. Comparison of drifting buoy velocities to HF radar radial velocities from the Ocean Networks Canada Strait of Georgia 25 MHz CODAR array. Can. Tech. Rep. Hydrogr. Ocean Sci. 319: vi + 38 p.

Les vitesses de courant à proximité de la surface ont été calculé à partir de bouées à la dérive déployé dans le Détroit de Géorgie, en Colombie Britannique, au Canada. Ces données ont été comparé à la vitesse radiale mesuré par deux systèmes de radar de haute fréquence, 25 MHz, dans le but de caractériser la précision et l'exactitude des données radars. Deux modes des bouées dérivantes ont été utilisé avec une profondeur d'échantillonnage véritable de 0.35 et 1.0 m, nous permettant d'étudier laquelle des deux bouées dérivantes correspond le mieux aux données radar.

La différence entre les vitesses mesurées a été quantifiée en utilisant les statistiques suivants : biais, l'erreur quadratique moyenne (EQM), le coefficient de corrélation linéaire (r^2) et la régression linéaire. Le biais de mesure, $\langle V_r^{radar} - V_r^{drifter} \rangle$, varie de 0 a -5 cm/s dépendant de la combinaison bouée dérivante/radar, ce qui signifie que les bouée dérivantes mesurent en moyenne une vitesse de courant plus élevée. L'EQM varie entre 11.3 et 17.2 cm/s, ce qui est élevé par rapport aux autres systèmes CODAR. Le coefficient de corrélation linéaire varie entre 0.46 et 0.81, ce qui reflète les valeurs EQM élevées. Les coefficients directeurs de droite, établies à partir des modèles de régressions linéaires, indiquent que les mesures faites par les bouées dérivantes profond et celles plus en surface sont respectivement 20% à 30% plus élevées que les mesures faites par radar. Cette différence augmente en parallèle avec la vitesse du courant.

Les bouées dérivantes à faible profondeur on systématiquement mesuré des vitesses de courant plus élevées comparé aux bouées dérivantes en profondeur, et celles-ci ont systématiquement surestimé les vitesses de courant mesuré à partir des radars, en dépit du fait qu'elles mesuraient la vitesse à une profondeur plus importante. Ceci suggère que les radars mesures seulement le champ de vitesse d'Euler, mais encore faut-il tenir compte des incertitudes de mesure mentionnées, ainsi que du fait que les vitesses mesurées par les radars peuvent démontrer un biais vers le bas dans le cas de vitesses élevées.

1 Introduction

In August 2012, Ocean Networks Canada installed the second of two high frequency (HF) oceanographic radar systems in the Strait of Georgia to measure surface currents in and around the Fraser River plume area (Fig. 1). These are commercially-available systems designed and built by CODAR Ocean Systems, USA. These systems are used, in conjunction with software provided by the vendor, to generate maps of surface currents over a rectangular grid with a nominal resolution of 1 km at hourly intervals.

As with any measurement, it is important to quantify the accuracy and precision of the HF radar current vectors. The vendor provides two quality metrics for this purpose. These estimates, called the spatial and temporal quality, are essentially the variance of the data which ultimately produce the hourly averages. While helpful, it is necessary to compare the data to independent velocity measurement to determine whether any bias exists, and to check if the temporal and spatial quality are reasonable.

In the case of the Strait of Georgia radar, the averaged velocity fields are thought to be plausible (Halverson and Pawlowicz, 2016), but in the hourly maps the actual accuracy is difficult to judge, as the Strait of Georgia's surface currents are complex, being affected by tides, wind, and river flow. In this data report we quantify the accuracy by analyzing drifter trajectories from a series of deployments that took place in the HF radar footprint. Surface drifters of two different designs were released, and their velocities were compared with those from the radar system.

1.1 Review of how HF radar measures currents

During the early development of radar systems, when the shortest wavelengths that could be created for electromagnetic radiation were tens of meters, it was noted that part of the received signal from over-ocean propagation seemed to be related to surface waves (Crombie, 1955). Further development of radar systems, driven primarily by military needs, quickly moved to shorter centimetre-scale wavelengths. However, numerous researchers proposed and demonstrated that high frequency radar systems (HF, i.e., 3 - 30 MHz frequency, 10-100 m wavelength) could be used to measure ocean surface currents and sea state (Hasselmann, 1971; Stewart and Joy, 1974; Barrick et al., 1977; Barrick, 1977).

HF radar systems estimate surface currents by analyzing spectrally the resonant scattering peak of the returned signal (or *echo*), which is often called the 1^{st}-order Bragg peak. The resonant scattering occurs when outgoing electromagnetic waves reflect from radially-propagating surface waves with twice the wavelength of the radar. Since ocean waves travel with a known speed set by the deep water gravity wave dispersion relation, the reflected signal is Doppler-shifted by a known amount. If, in addition, the waves are being advected by an underlying ocean current, then this Doppler shift is further modified. Thus, a measured Doppler shift is proportional to the sum of the known velocity of ocean waves and the unknown velocity of the surface current.

Radio waves in this frequency band propagate primarily as ground waves because they are effectively trapped on the electrically conductive ocean surface. Therefore, in principle, HF radar is capable of long range measurements beyond the horizon because

the waves follow earth's curvature. However, in practice, natural waters are lossy, and electromagnetic wave energy is lost by scattering and absorption, and also diluted geometrically, all of which reduce the signal to noise ratio and therefore the range and quality of the data.

A working surface-current radar system thus requires 1) a water body that is suitably conductive (i.e., salty), 2) the presence of ocean waves with a wavelength of half the radar wavelength, propagating in the radial direction, of amplitude large enough to generate a measurable reflection but not so large that most energy is scattered away, and 3) a method of localization so that a measured Doppler shift can be associated with a patch of ocean at a particular range and azimuthal direction. In practice, most seawater is salty enough to support propagation, and although surface wave spectra can be highly directional, there is generally enough wave energy in the radial direction to generate a suitable reflection. Range is easily found from time-of-flight estimates. However, obtaining directional information can be more challenging.

Conventional beamforming theory suggests that the angular resolution of an antenna array of width L, emitting radiation of wavelength λ, is about λ/L radians. Since ocean surface gravity waves suitable for this technique have wavelengths in the range of 10s of meters or more, implying even greater radar wavelengths, the size of an antenna array required to obtain even marginal angular resolution for azimuthal direction can be extremely large - upwards of 100 m. For example, in the Strait of Georgia, Bragg scattering from surface gravity waves with $\lambda = 6$ m (period, $T = 2$ s) requires electromagnetic radiation with a wavelength of 12 m, and to obtain an angular resolution of 6° the antenna array required is about 120 m across. This poses obvious logistical challenges. If only a single target is generating a return signal, then direction-finding techniques can be used with a much more compact antenna. Radar pulse timing separates targets by range, so the requirement is for only a single target at a given range, over all the azimuths returning signals. A simple surface current field can meet this requirement. If, for example, an ocean surface current is constant (say, moving eastward at 10 cm/s) over the radar field of view, which spans 180° of azimuth on a straight east-west coastline, then the radial component of this current at a fixed range would vary as 10 $\cos(\theta)$ where θ is the azimuthal direction, between a value of -10 cm/s in the up-current direction to +10 cm/s in the down-current direction. A particular radial speed, like 2 cm/s, would therefore appear only once in a 180° arc and would be a "single target" in the Doppler bin associated with speeds of 2 cm/s. If the current was moving southwards towards the coast, then all radial speeds would appear as two targets, equally spaced to the left and right of the radar, so that a direction-finding algorithm would need to separate two targets of variable relative power.

In CODAR, radar return directions are determined by combining the signals from one omnidirectional and two dipole antennas (oriented at 90° to each other). These dipole antennas are co-located with the omnidirectional antenna and hence the ground footprint of this antenna system is only a few tens of centimetres across. CODAR uses the MUSIC (MUltiple SIgnal Classification) algorithm (Schmidt, 1986) to provide the most likely direction for a maximum of two targets. The received spectrum of Doppler shifts are "binned" into a discrete set, each associated with a particular velocity (e.g., at -10 cm/s, -9 cm/s, -8 cm/s... +10 cm/s). By repeating the calculation for all Doppler bins at a

particular range, a plot of radial velocity as a function of azimuthal direction can be created, with one (or two) points for each velocity associated with each Doppler bin plotted at their most likely azimuth. This set of points, irregularly spaced in angular direction, is then smoothed and interpolated to find radial velocities at a fixed set of azimuths (say, every 5° of arc) for that range. The whole set of calculations is then repeated for all ranges to build up a radial velocity field. Various hardware power and digital computation efficiencies can be made by the use of transmitted signals that slowly sweep through a range of frequencies, and by applying Fourier transform processing techniques on the returned signal.

One disadvantage of the use of the MUSIC algorithm is that, although the mapping between the field of radial velocities and the antenna outputs is linear, the inverse mapping between the antenna outputs and the calculated field is highly nonlinear. It is therefore not clear how noise (errors) mathematically propagates through the algorithm, or indeed how one might characterize the the error of the resulting estimated velocity fields. The performance of the MUSIC algorithm has been found to be very good in specific examples, as long as the assumptions required (viz., maximum of two targets in a given range and Doppler bin) are correct. However, it may provide incorrect results when these assumptions are not met.

In addition, these radial velocities from two different antenna systems must be geometrically combined to obtain a full 2D current vector. The error in this combination is dependent on the system geometry. It is most accurate when the two radials are in perpendicular directions, and becomes less accurate as the two radials become co-linear. Furthermore, the area of the scattering patch increases with distance from the antenna, and the degree to which "sub-patch" variability is resolved depends on radial distance.

It would seem therefore that performance might depend on the field of radial velocities itself. For example, a constant current in a constant direction might be well-resolved, but a field containing eddies may be badly biased (although it is presumed that once the eddies are small enough they would be averaged out of the resulting velocity fields by the binning and smoothing operations in the algorithm). Thus it is possible that such systems might provide very useful results for some large fraction of the time when the velocity field is "simple" in some not-easily defined way, but may fail badly when the field becomes more complex. A validation exercise in one region of the ocean might not apply another, even if radar transmit frequencies, bandwidth, and in situ sampling techniques are consistent.

1.2 HF radar in situ validation

Although CODAR provides two statistical uncertainty estimates on each radial velocity (CODAR Ocean Sensors, 2013), independent validation is needed because the nature of HF radar measurement is somewhat different than other oceanographic current measurements.

Measured velocities from acoustic Doppler current profilers (ADCPs), or derived velocities from GPS-tracked drifting buoys most frequently serve at the reference. ADCP comparisons have the advantage in that they are fixed in space (i.e., moored) for a significant period of time, thereby making a long time series comparison possible. The

disadvantage is that HF radar measurements represent exponentially weighted averages of the upper few meters of the water column, and ADCP side-lobe interference restricts ADCP measurements to deeper depths. This limitation is particularly restrictive in most of the present study area, where a bottom-mounted ADCP in deep water would be able to measure only up to within about 20 m of the surface. Shear, enhanced by the strong near-surface stratification, and the shallow HF radar effective sampling depth of about 50 cm, would then make the current velocity comparison meaningless.

The advantage of using drifters is that they can be designed to sample shallow depths, and because they are Lagrangian they can drift freely throughout the HF radar footprint. A comparison done this way provides a bulk estimate of HF radar uncertainty, although one could argue it obscures systematic direction-finding problems. Ohlmann et al. (2007) demonstrate how to characterize a particular cell with repeated drifter deployments.

Previous studies comparing CODAR radial velocities to drifter-derived radial velocities have found Root Mean Square (RMS) differences ranging from 1.4 to 13.3 cm/s, and bias values ranging from -9.3 to 10.7 cm/s ($V_r^{radar} - V_r^{drifter}$) (Ohlmann et al., 2007). Paduan et al. (2006) calculate RMS differences of 10.0 to 12.7 cm/s. Bias values of -4 to -1 cm/s ($V_r^{drifter} - V_r^{radar}$) and RMS differences of 6 to 10 cm/s were measured by 25 MHz systems by Rypina et al. (2014). Lipa et al. (2009) measure RMS differences of 8.5 cm/s. Hubbard et al. (2013) compare drifter velocities to radial velocities from four different 42 MHz systems, and calculate RMS differences of 8.67 to 14.36 cm/s, and bias values of -7.05 to 2.64 cm/s ($V_r^{drifter} - V_r^{radar}$).

Although none of these studies may be directly applicable to the Strait of Georgia HF radar system because of differences in operating frequency, oceanographic environment, or instrument configuration, they suggest that the hourly current fields are likely to have random errors as as high as 15 cm/s, and biases as high as ± 5 cm/s. Random oceanographic noise and instrumental errors can be reduced by averaging. Bias, however, will remain even after averaging.

The analysis of Halverson and Pawlowicz (2016) suggests that the internal consistency of the measurements, at least when averaged, indicate that the Strait of Georgia CODAR system provides a reasonably accurate picture of surface currents. For example, the long-term average current vectors reveal an anticyclonic gyre fed by buoyant water from the Fraser River mouth, and the current vector orientation follows the prevailing wind direction. Both the tidal currents and the currents near the river mouth were weaker than expected, however. The largest average current speed in the SoG CODAR footprint is 14 cm/s, which occurs at the river mouth. The surface tidal currents are roughly half of the speed of the barotropic tidal currents.

2 Study site, materials, and methods

2.1 Strait of Georgia and the Fraser River plume

The Strait of Georgia (hereafter SoG) is a mid-latitude semi-enclosed coastal basin about 200 km in length, between 20 and 40 km wide, situated between mainland British Columbia and Vancouver Island. It is a relatively deep, fjordâĂŞlike system with signif-

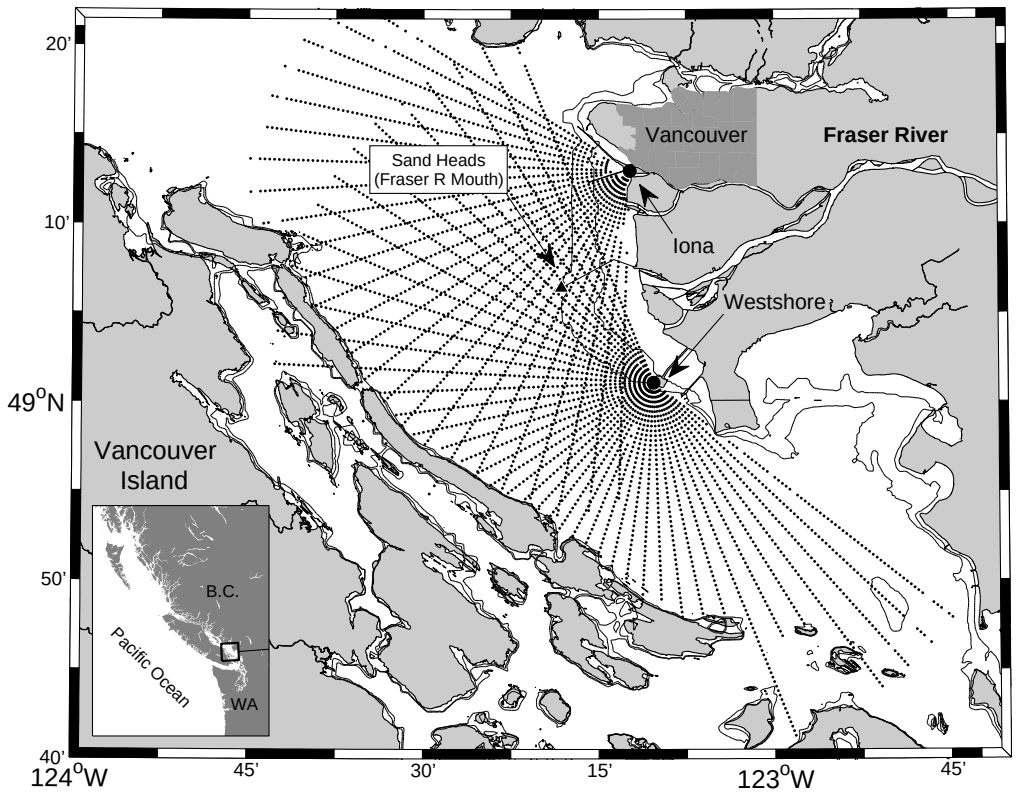

Figure 1: Map of the lower Strait of Georgia illustrating the idealized radial grids for the Iona and Westshore CODAR sites.

icant entrances to the Pacific Ocean at its northwest end via Johnstone Strait and its southern end via Juan de Fuca Strait.

Fresh water from the Fraser River discharges directly into the HF radar footprint near the city of Vancouver, Canada (Fig. 1), forming a buoyant and usually turbid, brackish plume, extending for 20 km or more from the river mouth in a surface layer some 5 to 10 m thick (Halverson and Pawlowicz, 2011). At any given time, the plume consists of the accumulation of about 2 days of tidally-pulsed river outflow, mixed with saline SoG water (Halverson and Pawlowicz, 2011). The mean salinity in the plume is highly correlated with river flow at subtidal frequencies, such that high flow river flow results in a relatively fresh plume (Royer and Emery, 1982; Halverson and Pawlowicz, 2008). Superimposed on the low-frequency salinity response to river flow are relatively large fluctuations driven by the tides, which are modulated by the $\approx$14 day spring/neap cycle and by the lunar declination cycle (Halverson and Pawlowicz, 2008). Northwesterly winds can advect the plume down the strait to the southeast, while southeasterly winds advect the plume up the strait to the northwest (Royer and Emery, 1982; Halverson and Pawlowicz, 2016; Pawlowicz et al., 2017).

Fraser flow is uncontrolled by dams and the annual discharge cycle is characterized by high flows during a summer freshet resulting from summer melting of the BC interior

snowpack, and much lower flows in winter. However, fall/winter rainfall events over the smaller coastal drainage basins downstream of Hope can add a substantial amount of fresh water for short periods.

Tides in the SoG are of the mixed type and characteristic of the temperate eastern Pacific. Within the CODAR footprint for the data in this study, tidal currents are strongest near the Fraser River mudflats, reaching 25 cm/s for M_2 , but are generally 15 cm/s or less elsewhere (Halverson and Pawlowicz, 2016). There is a considerable spatial variability in the phase difference between the sea surface elevation and currents, suggesting that baroclinic effects are important.

2.2 Ocean Networks Canada HF radar

The Ocean Networks Canada (ONC) VENUS ocean observatory maintains an array of CODAR Ocean Sensors SeaSonde units in the southern Strait of Georgia. At the time the fieldwork was undertaken for this study, only two sites were in operation: one located on shore at the Iona Beach regional park (VION), and a second located on the Roberts Bank Superport at the Westshore coal terminal (VCOL) (Fig. 1). The units operate at a nominal frequency of 25 MHz (radio wavelength of 12 m), giving Bragg resonance with surface gravity waves of 6 m wavelength. Such waves travel at 3 m/s in deep water.

Raw antenna time series are processed to radial velocities with the radial site CODAR processing software. The SeaSonde units produce "hourly" radial current maps by combining (ideally) seven 10 min averages. Each map is gridded to range bins of 0.5 km and bearing bins of 5âĂŃ°. Angular gaps less than 15°in width are filled by interpolation. The nominal maximum range for the radial maps is 40 km. Targets over land are flagged, but removed for this study. The maximum current speed allowed by the 1st-order line detection algorithm, *CurrentVelocityLimit*, was 85 cm/s at Westshore, and 180 cm/s at Iona. The minimum Bragg signal to noise ratio necessary for a radial velocity computation, *RadialBraggNoiseThreshold*, was 4 (6 dB). Additional instrument settings are summarized in Appendix A with example hourly radial headers from both sites.

Conductive media within a wavelength of the antenna can distort the idealized beam patterns, which in turn can produce an error in inferred bearing angles, causing radial velocities to be improperly georeferenced (Barrick and Lipa, 1999). In practice, distortions in the beam pattern are accounted for by measuring beam patterns using a test transmitter in a boat. Corrected response patterns are applied during the processing of both radial sites.

The range over which surface ocean information can be measured varies with time because of environmental factors and radio frequency noise, both of which determine the signal to noise ratio of the measured echo (Shearman, 1983). The three environmental factors that impact the working range over which reliable radial current measurements can be made in the SoG HF radar system are sea water conductivity, sea state, and tides (Halverson et al., 2017). Of the three, conductivity has largest impact because of the large variations in near-surface salinity caused by seasonal fluctuation in Fraser River discharge. The second most important factor is sea state, which is governed primarily by wind. Finally, working range varies with the tide. The effect is very weak at Westshore,

however, tidal fluctuations are particularly acute at Iona because this site overlooks tidal mudflats which, when exposed at low tide, attenuate a large proportion of energy. In fact, when the river flow is high in early summer, and the tide is low, the working range for current measurements at Iona rarely exceeds 10 km.

2.3 Meteorological and tidal data

The nearest source of meteorological data to the Fraser River plume is the Sand Heads lighthouse station, Environment Canada Climate ID #1107010, which is positioned at the end of the jetty extending from Steveston to the edge of the mudflats (Fig. 1). The hourly wind speed is a two minute average measured at an elevation of 11 m.

We chose to use the wind measurements at Sand Heads to represent the wind conditions over the sampling region because of its proximity and because the lightstation is built on pilings some 6 km from shore, and is therefore essentially a marine measurement. Other nearby stations could also suffice, such as Vancouver Airport or Halibut Bank, since the measured wind at these stations co-varies with Sand Heads closely except for the influence of some local orographic effects.

Tidal heights used in this paper were those predicted for Point Atkinson, BC, located 25 km north of the Fraser River mouth. Tidal records are available closer to the river mouth, but we sought a time series uncontaminated by the river stage.

2.4 Drifters

2.4.1 Pacific Gyre Microstar 1 m drogues

The 1 m drogued drifters in this study were manufactured by Pacific Gyre. The drifters consist of a surface buoy and a drogue connected by a short tether (Fig. 2). The 20 cm diameter ABS plastic surface buoy houses all of the electronics and the battery. The GPS position is sent to Pacific Gyre's data servers at 5 min intervals. The communications are housed inside the surface buoy. The units are user serviceable, and sampling rates can be adjusted in situ from a web interface. A ⅛" Amsteel-Blue tether connects the buoy to the drogue. The drogue design is based on corner radar reflectors, and are made out of a polyester fabric. It is 1.20 m in both height and width, and the centre of the drogue rests at a depth of 1 m. Therefore the depth range sampled by the drogue is 0.4 m to 1.6 m. The water-following capabilities of this drifter were evaluated with the use of drifter-mounted acoustic current meters. Ohlmann et al. (2005) showed that there is a "slip" velocity of about 1 to 2 cm/s that is aligned with the direction of the surface waves.

The Microstar drifters sample GPS position and sea surface temperature at 5 min intervals and relay the data back to the vendor's data servers via Iridium telemetry. Users then log on to the Pacific Gyre website to download data in a number of formats. Pacific Gyre also provides a Google Map interface so that users can track the position of their drifters in real time, which proved to be very useful feature because it simplifies recovery at sea.

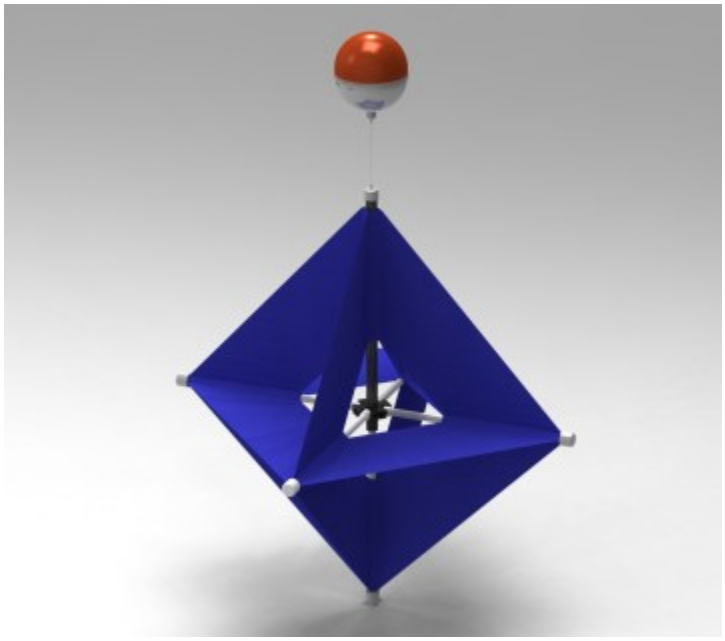

Figure 2: Pacific Gyre Microstar drifter. The radar corner reflector style drogue is centred at 1 m depth. The drogue itself is 120 cm wide, and is fully collapsible.

2.4.2 IOS Surface Current Trackers

The second type of drifter used in this experiment is the Surface Current Tracker (SCT), designed and built by Tamás Juhász and Charles Hannah of the DFO Institute of Ocean Sciences. The electronics for GPS location and data transmission are packaged in a small consumer grade asset tracker manufactured by SPOT LLC called the Trace^{TM}. The asset tracker uses Iridium communications to relay the 5-min GPS fixes (configurable) to SPOT's servers. The SCT buoy is 37.5 cm in height, and the sponge is 7.5 cm thick and 23 cm in diameter. When in the water, 3 to 5 mm of the sponge rides above the water surface. The Trace is designed to enter a low power sleep mode when it is not in motion, but calm seas do not cause enough "jiggling" to wake the sensor. To remedy this, the unit is mounted on top of a spring (actually a door stop) to keep it in motion.

2.5 Drifter deployment strategy

Clusters of drifters were released on numerous occasions over the period of 19 to 21 Sep 2014. The drifters were deployed for 6 to 24 hours or more, however they did not necessarily stay within the radar footprints over the full deployment. Most of the drifters were recovered by a small vessel and re-released in the radar sampling footprint. Most of these releases were made from the R/V Tully during an Ocean Networks Canada maintenance cruise. Nearly all drifter releases occurred directly west of the Sand Heads lighthouse in the centre of the strait (Fig. 1). In many cases, both drifter types were deployed simultaneously to provide a robust way to compare their relative water-following capabilities, and to assess which drogue style compares more closely with HF radar

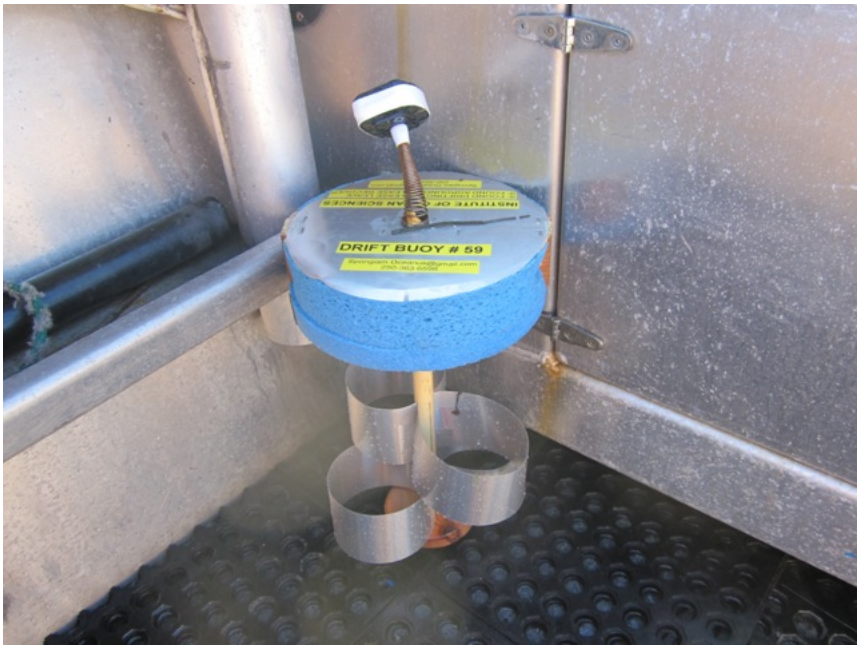

Figure 3: Surface Current Tracker (SCT) buoy built by the Institute of Ocean Sciences. The total draft of the unit is 37.5 cm. Buoy communications are handled by a small commercially available SPOT asset tracker mounted on top of a door stop. The asset tracker uses Iridium communications to relay the GPS fixes to SPOT servers.

current measurements.

2.6 Calculation of drifter radial velocity from drifter trajectories

A single HF radar site measures line-of-sight velocities which are commonly referred to as 'radials'. We choose to compare drifter velocities to radial velocities because radial velocities are more fundamental; whereas 'total' velocities (U, V) are derived by combining radial velocities from multiple HF radar sites. The first step required to calculate a drifter 'radial' velocity is to compute the U and V velocities with a centred finite difference of consecutive GPS positions and times. To compute radial velocities, the drifter velocities were then projected on to the vector connecting the radar radial cell closest to the drifter and the radar station. The angle of this vector is the bearing of the radial grid cell. The sign convention is such that a positive radial velocity indicates flow toward the radar site, while a negative velocity indicates flow away from the radar site.

The drifter sampling rate is 5 min, while the radar computes hourly radials from a series of short term (10 min) radials. This means that a single drifter can produce multiple velocity estimates within a given radar radial cell in a 75 min period. However, unlike in other studies (e.g., Rypina et al., 2014), the drifter data were not averaged to match the radar averaging windows, which means that it is possible to get a sense of the variability occurring on sub-grid and sub-averaging period scales.

2.7 Comparison statistics and model fitting

The basic aim sought by comparing the drifter and HF radar velocities is to determine the accuracy (i.e., bias) and precision (i.e., variance) of the HF radar measurements. In this study bias is simply the average difference between the measurements,

$$\langle V_r^{radar} - V_r^{drifter} \rangle, \tag{1}$$

and the variance is quantified by the RMS error or mean squared deviation,

$$\sqrt{\langle (V_r^{radar} - V_r^{drifter})^2 \rangle}. \tag{2}$$

Regressions are used to quantify the relationship between drifter-derived radial velocity and HF radar velocity. When comparing the two measurements it is helpful to define the ideal result (however unrealistic), and then contextualize the results as the deviation from the ideal comparison. We choose the ideal comparison to be the one where the measured currents from each instrument agree perfectly, meaning a regression of the two measurements would produce a straight line with a slope of unity and no offset. Scatter from unresolved motion or instrument noise would be distributed evenly about $y = x$. Assuming for this comparison that the drifter velocities represent the true ocean currents, the linear model we are using is

$$V_r^{drifter} = a + bV_r^{radar} + \epsilon \tag{3}$$

where a and b are unknown coefficients, and ϵ is the error term. Therefore we seek to quantify the relationship between the drifter and radar currents with a simple linear model. The regression is written this way because we are assuming that the CODAR measurements must be scaled to represent the actual currents.

Before fitting a linear model, we should consider how errors in both the drifter and CODAR measurements are treated by the fitting process. The fitted parameters a and b depend on how the errors are handled by the fit.

As discussed in the introduction, RMS differences between radar radial velocities and drifter-derived velocities are as high as 13 cm/s (Section 1.2). The uncertainty reflects both unresolved oceanographic spatiotemporal variability, and instrumental uncertainty, such as might be caused by direction-finding errors. While CODAR provides radial data quality metrics, it is not clear if these accurately reflect the instantaneous uncertainty, i.e., the uncertainty on an hourly averaged radial velocity. Thus for this work we simply assume that each radar measurement has the same error. There is also uncertainty in the drifter GPS positions, which when used to compute velocity might introduce non-negligible errors because of the first order finite difference scheme. Drifters are sensitive to Stokes drift, but it is not clear if this is also true for HF radar (Sec. 4.3.1). Windage might also cause variability in the drifter velocities that is not measured by HF radar, and if this is true it would be more significant for the shallow SCT drifters than the deeper Microstar drifters. As with the radar measurements we assume that all drifter-derived velocities have the same uncertainty.

The familiar ordinarily least squares (OLS) approach to curve fitting assumes the y-variable contains uncertainty, however, as discussed above, both the drifter and radar

velocities are expected to contain uncertainty. Therefore we choose to use total least squares (TLS) minimization, a technique which allows for errors in both variables. In TLS, the optimal solution is the one which minimizes the distance from each point to the best-fit line. This line is often determined by a singular value decomposition (SVD). For reference we also include the best fit lines from regressing both y on x, and x on y, using OLS. The slope of the TLS solution always lies in between the OLS solutions. The OLS slopes are included in each of the four permutations of radar site and drogue style.

3 Results

3.1 Weather, tides, and Fraser River flow

The wind exhibited three major patterns during the three day sampling period (Fig. 4a). On the first day, the wind originated from the southeast at speeds reaching 7 m/s. The wind then shifted to northwesterly at up to 7 m/s the next day. On the last day, during the final 12 hours of the experiment, the wind was weak and variable. The tides followed a diurnal pattern of large ebb $\rightarrow$ large flood $\rightarrow$ weak ebb $\rightarrow$ weak flood, and the first drifter release occurred at the start of a large ebb (Fig. 4b). The Fraser River discharge as measured at Hope was relatively steady at about 1500 m^3/s (not shown), while the discharge at the mouth, estimated using the methods based on Halverson et al. (2017), was about 2100 m^3/s.

3.2 SCT/Westshore comparison

In this section we compare velocities derived from the SCT drifter trajectories to the radial velocities measured by the Westshore CODAR station. The drifters were largely contained in the northern part of the Westshore domain (Fig. 5). For this comparison there were a total of 1765 drifter velocity measurements and 381 radar estimates.

A scatter plot of radar radial velocity against drifter radial velocity shows that the data are positively correlated, and reasonably close to the 1:1 line (Fig. 6). The total least squares fit of the linear model $V_r^{drifter} = a + b * V_r^{radar}$ yields a slope $a = 1.32$ and an offset of $b = 2.36$ cm/s. As expected, the slope is bracketed by both OLS fit slopes.

The bias, defined as the average of the radar radials minus the drifter radials, is -0.01 cm/s, and the RMS difference is 14.3 cm/s. A histogram of the difference between the radar radials and the drifter radials is fairly well approximated by a Gaussian distribution (Fig. 6b), indicating that the errors, whether instrumental, oceanographic, or both, are mostly random. The centroid of the distribution is -0.50 cm/s, while the standard deviation is 16.4 cm/s.

3.3 Microstar/Westshore comparison

In this section we compare velocities from the Microstar drifters to the radial velocities measured by the Westshore CODAR station. The release locations and times were very

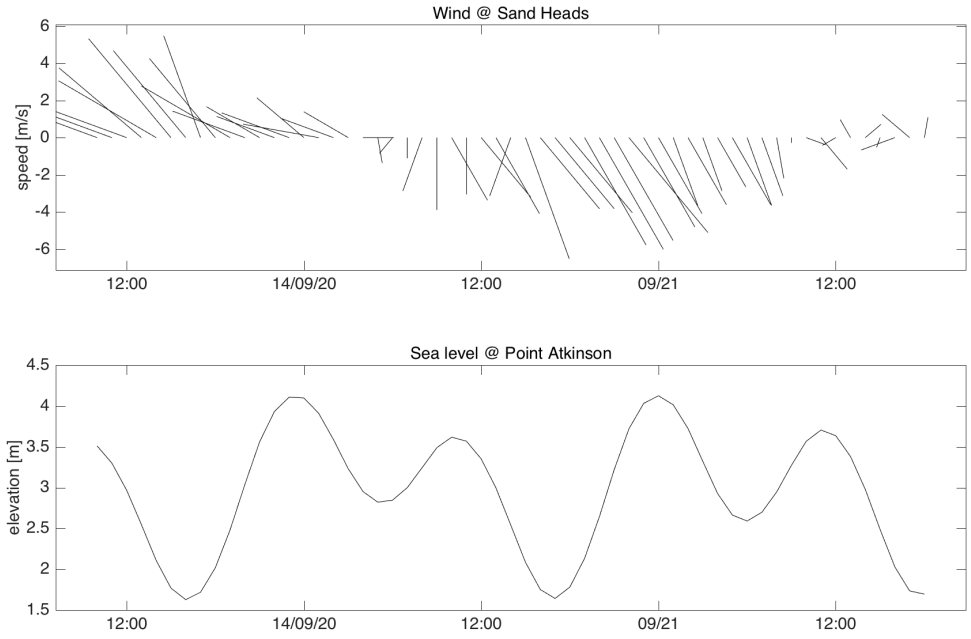

Figure 4: a) Stick-plot of wind speed and direction recorded at the Sand Heads light station (Fig. 1) and b) predicted tides at Point Atkinson.

similar to the release locations and times of the SCTs because both drifter styles were often released in tight clusters (Fig. 5).

For this comparison there are 2072 drifter velocity measurements and 679 radar estimates. A scatter plot of radar radial velocity against drifter radial velocity shows that the data are positively correlated, and reasonably close to the 1:1 line (Fig. 8a). A least squares fit to a linear model yields a slope of $a = 1.20$ and an offset of $b = 4.54$ cm/s.

The average value of the radar radials minus the drifter radials is -3.43 cm/s, and the RMS difference is 15.4 cm/s. A histogram of the difference between the radar radials and the drifter radials is fairly well approximated by a Gaussian distribution (Fig. 8b). The centroid of the distribution is -2.11 cm/s, while the standard deviation is 16.3 cm/s. There is a disproportionately high number of occurrences in the range of -30 to -50 cm/s (high drifter speeds and/or low radar speeds), which deviate significantly from the Gaussian fit. These points will be discussed in Section 4.1.2.

3.4 SCT/Iona comparison

In this section we compare velocities from the SCT drifters to the radial velocities measured by the Iona CODAR station. The release locations and times are identical to the releases used in the SCT/Westshore comparison (Fig. 9). The comparison includes 1674 drifter velocity measurements and 255 radar estimates.

A scatter plot of radar radial velocity against drifter radial velocity shows that the

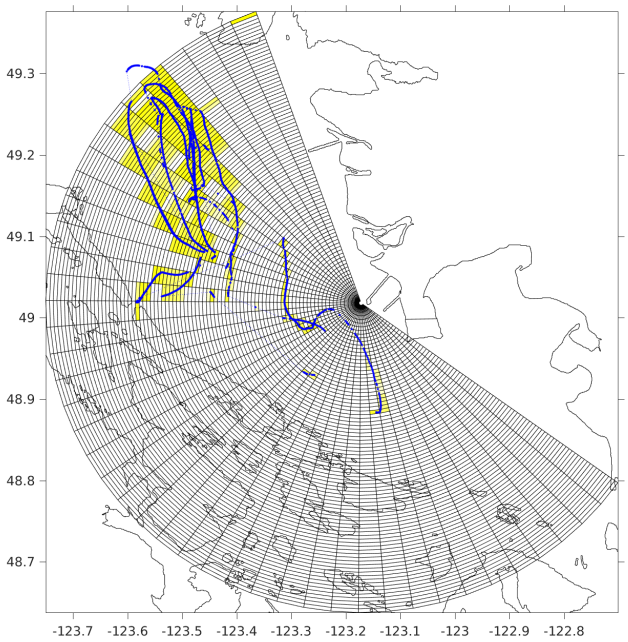

Figure 5: Map illustrating the SCT drifter tracks relative to the Westshore radial grid. Radial cells filled with yellow indicate cells from which radial velocities were extracted.

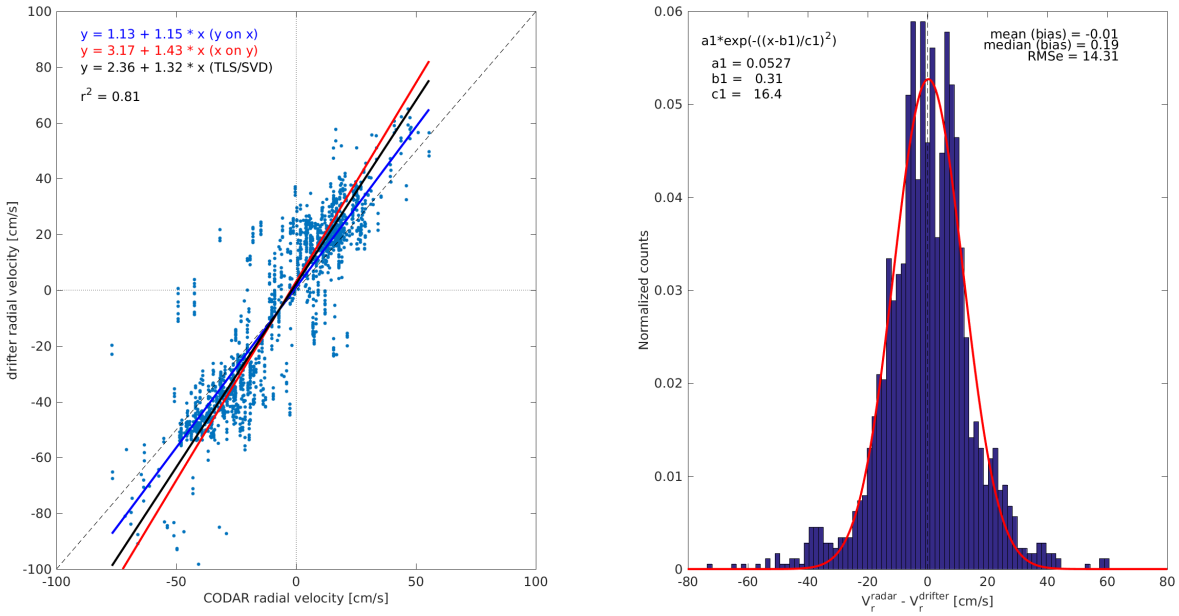

Figure 6: a) Scatter plot of Westshore HF radar radial velocity and SCT drifter-derived velocity and b) PDF of the difference between the radar and drifter radial velocities.

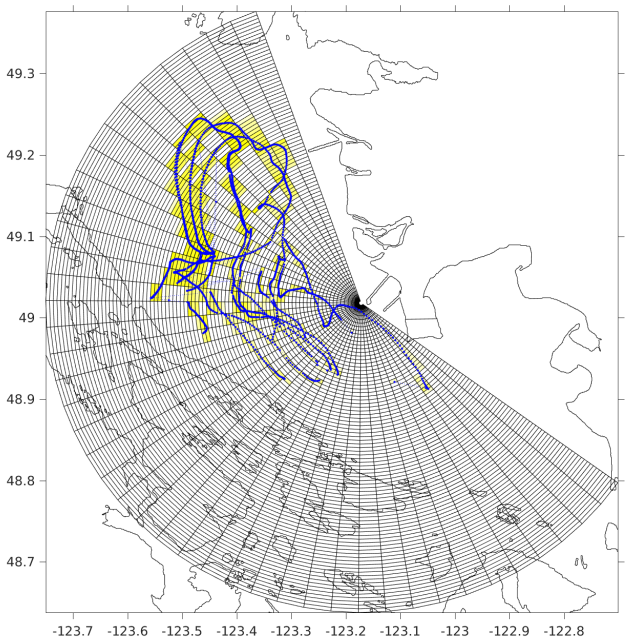

Figure 7: Map illustrating the Microstar drifter tracks relative to the Westshore radial grid. Radial cells filled with yellow indicate cells from which radial velocities were extracted.

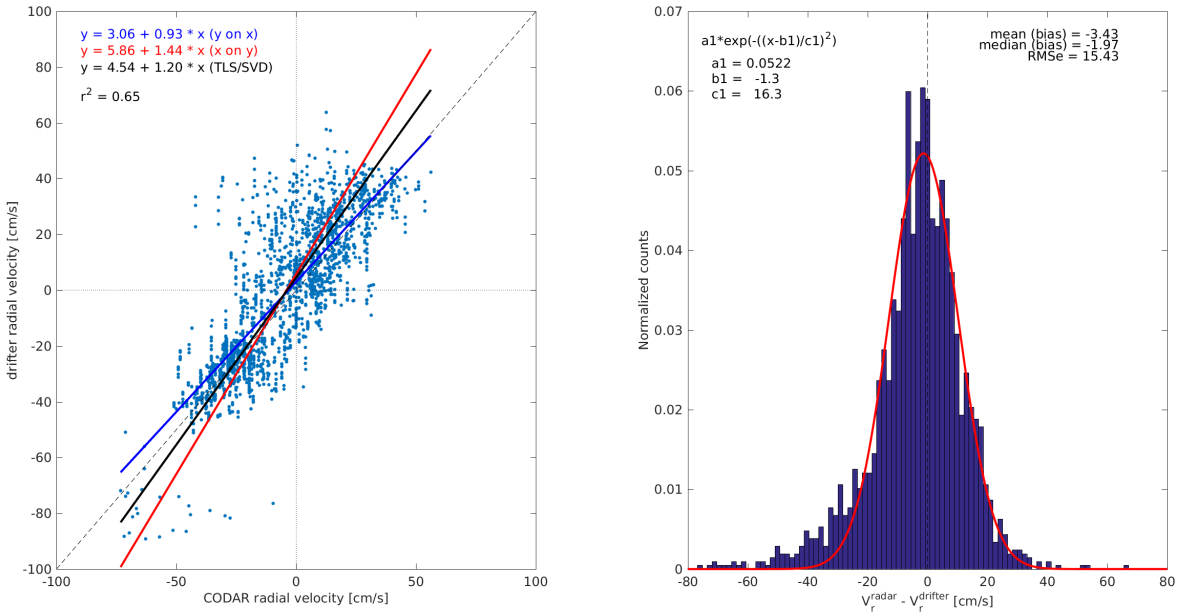

Figure 8: a) Scatter plot of Westshore HF radar radial velocity and Microstar drifter-derived velocity and b) PDF of the difference between the radar and drifter radial velocities.

data are positively correlated and reasonably close to the 1:1 line (Fig. 10a). A least squares fit to a linear model yields a slope of 1.31 and an offset of 4.27 cm/s.

The average value of the radar radials minus the drifter radials is -3.09 cm/s, and the RMS error is 11.3 cm/s. A histogram of the difference between the radar radials and the drifter radials is fairly well approximated by a Gaussian distribution (Fig. 10b). The centroid of the distribution is -3.48 cm/s, while the standard deviation is 13.6 cm/s. There is a disproportionately high number of occurrences in the range of -25 to -35 cm/s (high drifter speeds and/or low radar speeds), and also some instances of high positive values ($V_r^{radar} - V_r^{drifter} > 30$ cm/s). These points occur in sufficient numbers to impact the bulk statistics, and will be discussed further in Section 4.1.2.

3.5 Microstar/Iona comparison

In this section we compare velocities from the Microstar drifters to the radial velocities measured by the Iona CODAR station. The release locations and times are identical to the releases used in the SCT/Iona comparison (Fig. 11).

The comparison includes 1338 drifter velocity measurements and 370 radar estimates. A scatter plot of radar radial velocity against drifter radial velocity shows that the data are positively correlated (Fig. 12a). A least squares fit to a linear model yields a slope of 1.52 and an offset of 3.70 cm/s.

The average value of the radar radials minus the drifter radials is -2.19 cm/s, and the RMS difference is 17.2 cm/s. A histogram of the difference between the radar radials and the drifter radials, $V_r^{radar} - V_r^{drifter}$, is fairly well approximated by a Gaussian distribution (Fig. 12b). The centroid of the distribution is -6.87 cm/s, while the standard deviation is 15.2 cm/s. There is a disproportionately high number of occurrences in the range of 15 to 60 cm/s relative to a Gaussian distribution, which is caused by a large number of high negative drifter radial speeds combined with low radar radial speeds. There is a slight deficit of velocity differences in the range of -30 to -40 cm/s.

4 Discussion and conclusions

Table 1 summarizes the statistics from each of the four possible comparisons that could be made with two drifter styles and two radar sites. There are some differences between the drifter/radar pairs, and the remainder of the discussion is devoted to what the differences imply about the measurements, their errors, Stokes drift, and near-surface flow in the Strait of Georgia.

4.1 Bias and linear regression results (i.e., accuracy)

4.1.1 Bulk characterization of all four comparisons

Among all four possible comparisons, the average deviation between the radar speeds and the drifter speeds, or bias, ranged from -0.1 cm/s to -3.43 cm/s, suggesting a tendency for the drifter speeds to be higher. The median difference was also computed to reduce

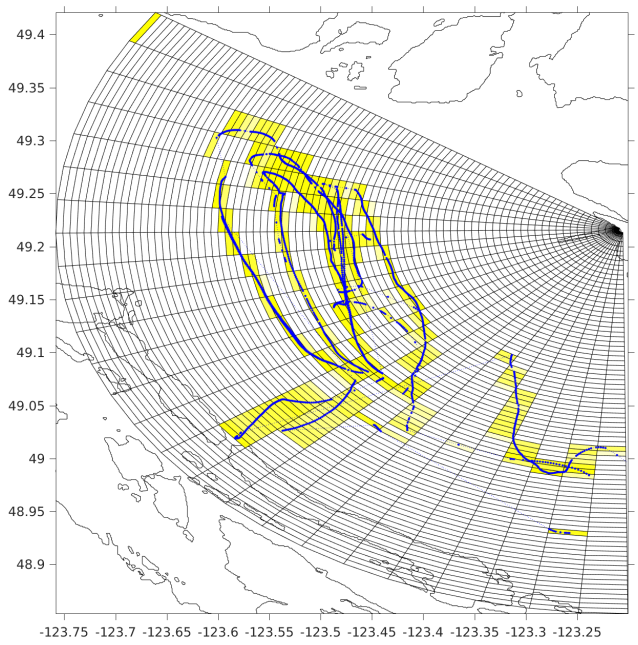

Figure 9: Map illustrating the SCT drifter tracks relative to the Iona radial grid. Radial cells filled with yellow indicate cells from which radial velocities were extracted.

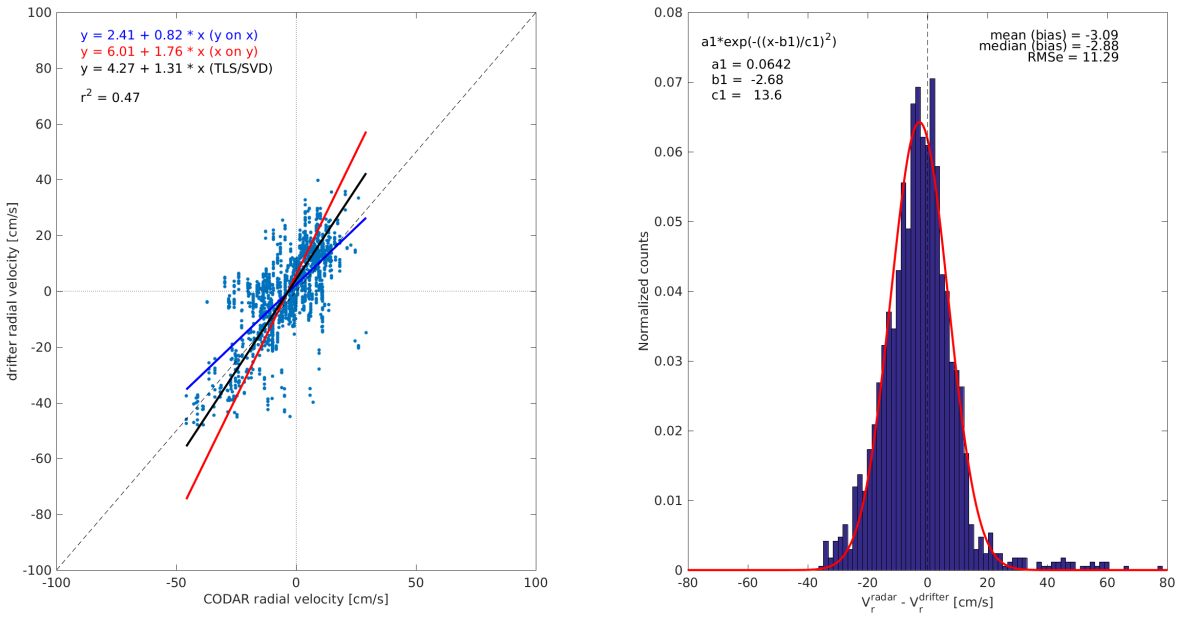

Figure 10: a) Scatter plot of Iona HF radar radial velocity and SCT drifter-derived velocity and b) PDF of the difference between the radar and drifter radial velocities.

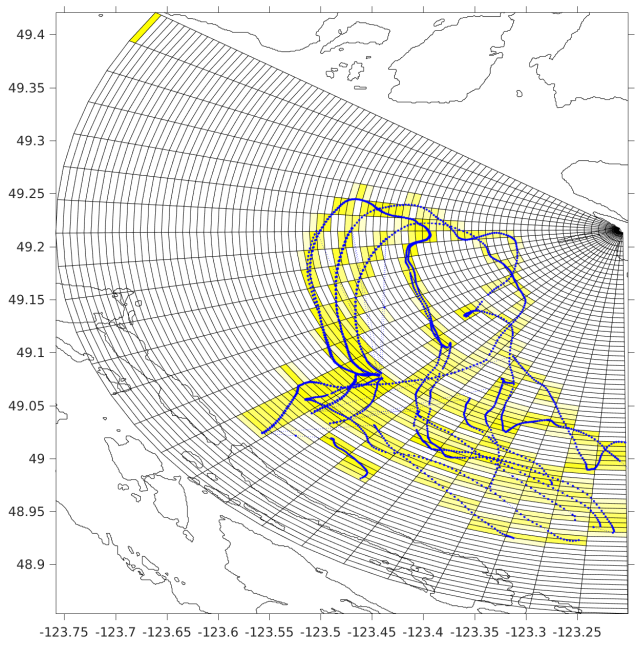

Figure 11: Map illustrating the Microstar drifter tracks relative to the Iona radial grid. Radial cells filled with yellow indicate cells from which radial velocities were extracted.

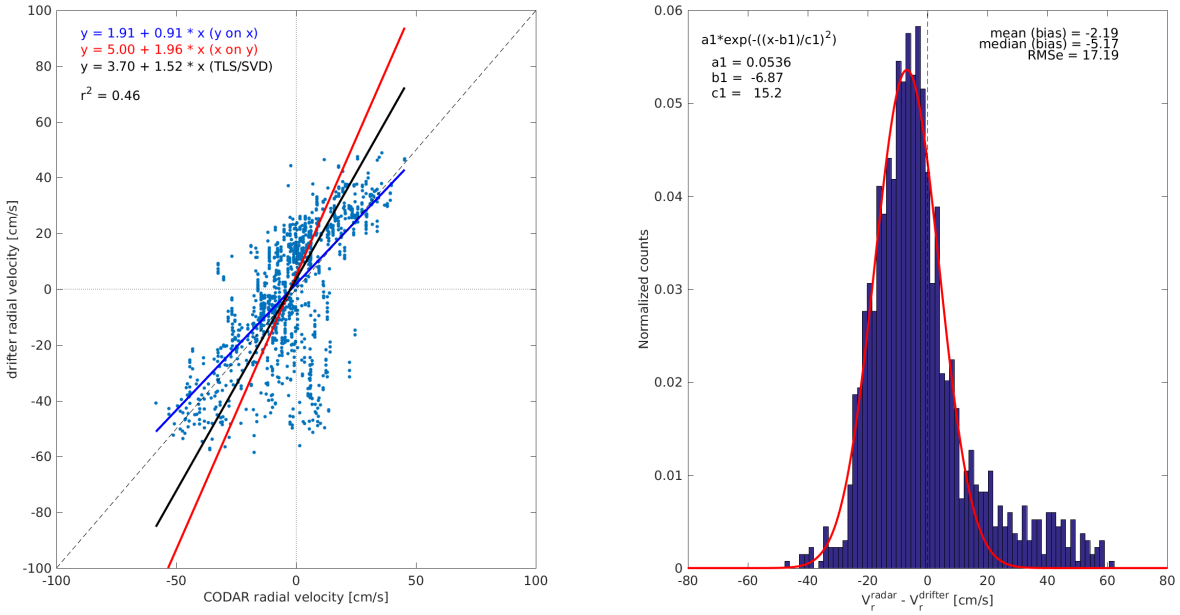

Figure 12: a) Scatter plot of Iona HF radar radial velocity and Microstar drifter-derived velocity and b) PDF of the difference between the radar and drifter radial velocities.

	$V_r^{drifter} = a + b * V_r^{radar}$	bias (mean)	bias (median)	RMS diff	r^2
SCT/Westshore	a = 2.36, b = 1.32	-0.01	0.19	14.3	0.81
Microstar/Westshore	a = 4.54, b = 1.20	-3.43	-1.97	15.4	0.65
SCT/Iona	a = 4.27, b = 1.31	-3.09	-2.88	11.3	0.47
Microstar/Iona	a = 3.70, b = 1.52	-2.19	-5.17	17.2	0.46

Table 1: Summary statistics for all four drifter/CODAR comparisons. The bias convention is $\langle V_r^{radar} - V_r^{drifter} \rangle$, and all quantities have dimensions of cm/s except for the regression slope, b, and squared correlation coefficient, r^2, which are both dimensionless.

the influence of outliers, and while it can differ from the bias by a few cm/s, the overall trend is also that the drifters measure higher velocities.

It is not clear, however, that the difference in the bias values among the drifter/radar pairs is meaningful. We will show later that some of the RMS estimates are sensitive to outlier points. In other words, the estimated bias and RMS values were not robust to outliers, and so although it is likely that the drifters generally report a faster velocity (a conclusion supported by the linear regression), we do not have statistical confidence in the degree of difference indicated by the bias estimates.

The comparison of the HF radar radial velocities to the drifter velocities was modelled with a simple straight line and offset, where the coefficients were empirically determined by a TLS fit. The slopes obtained from these fits ranges from 1.20 to 1.52 depending on which pair of instruments is compared. The magnitude of the slopes indicates that the flow as measured by the drifters is faster by about 20% or more. A regression slope of more than one also means that the difference in speeds measured by the instruments increases linearly with flow speed.

The conclusion that the drifters measure faster flow speeds is largely independent of the fitting method. In nine out of the twelve fits (three fits per instrument pair), the fitted slope is greater than one. The remaining three yielding a slope less than one were the following "y on x" cases: Microstar/Iona, Microstar/Westshore, SCT/Iona. Although the conclusion that the drifters report a faster flow than the radar is firmly supported by the data, there is a wide range in the fitted slopes: 0.82 to 1.96. This variability highlights the importance of outliers and how measurement errors are considered by the fitting method.

In some cases, the residuals remaining after removing the linear trend indicate some higher-order dependence on flow speed, however there is not much consistency between the four comparisons. It is important to stress that there is no reason to expect a linear increase in velocity difference. A simple linear model was chosen in light of the relatively large scatter; more sophisticated models could not be justified in the absence of physical arguments. The HF radar in this study sample a region of considerable complexity. The surface waters contain strong non-linear internal waves, multiple fronts, and variable stratification. Stokes drifts varies with sea state, and therefore wind speed, fetch, and duration. In Section 4.3.1 we discuss some of these issues.

4.1.2 Cross-comparison of radar stations for a given drifter

Here we examine how each radar compares to a particular drifter type to see if the radar stations measure consistent velocities. The expectation is that the comparison between a particular drifter type (e.g., Microstar) and each radar will produce identical relationships because both HF radar are short range 25 MHz systems with similar configurations. Any difference might indicate that the two radars perform differently.

In the case of the SCT drifters, the slope and offset of the comparison with Westshore is 1.32 and 2.36 cm/s, respectively, while the slope and offset of the comparison to Iona is 1.31 and 4.27 cm/s (Table 1). In other words the slopes are nearly the same, while the offset is 2 cm/s larger for Iona. In light of the relatively large amount of scatter in the comparisons, the difference in offset is likely not significant.

In the case of Microstar drifters, the slope and offset of the comparison with Westshore is 1.20 and 4.54 cm/s, respectively, while the slope and offset of the comparison to Iona is 1.52 and 3.70 cm/s (Table 1). The difference in slopes is such that the Iona radial speeds must be scaled by a larger number to match the drifters, which are assumed to represent the true flow speed. In other words, Iona evidently underestimates the true flow to a greater degree than Westshore by about 15%. The offset for Iona is higher, meaning that Iona measures the flow to be slightly faster than Westshore at low flow speeds.

Thus, the Microstar drifter comparison indicates that the two radar systems do not produce equal measurements of the same water speed, while the SCT comparison indicates that both radar systems measure consistent speeds. How is this resolved? The answer is that statistical outliers have a significant impact on the summary statistics. In particular, there are a series of high residual values in both Microstar comparisons (Figs. 8b and 12b). These outliers were the result of HF radar measurements that were much lower than the drifter velocities. The outliers occurred in large enough quantities to affect the least squares fitting procedure. For example, if we disregard points in the Microstar/Iona comparison for which $V_r^{radar} - V_r^{drifter} > 25\,\mathrm{cm/s}$, and fit a line to the scatter plot using the TLS method, then the linear relationship has a slope of 1.23. This value is closer to the slope of the Microstar/Westshore regression (which also contains outliers, however, they do not dramatically impact the curve fitting). Thus, we conclude that the radars themselves measure currents in a statistically consistent way.

4.1.3 Cross-comparison of drifter styles for a given radar station

We can also phrase the drifter/radar statistics in such a way as to determine if the drifter drogue style alters the comparison to HF radar. In this case, we compare both drifter types to a particular HF radar site.

The mean and median bias in the Westshore comparisons are more negative for the Microstars than the SCTs, suggesting that the Microstars tend to travel faster than the SCTs for a given radar measurement. The same is true for the Iona median bias, but not the Iona mean bias. However, as discussed earlier in Sections 4.1.1 and 4.1.2, the Iona/Microstar statistics were affected by outliers so we instead focus on what what the linear regressions (with outliers removed) can tell us.

For the comparisons to Westshore, the slope and offset of the Microstar comparison is

1.20 and 4.54 cm/s, respectively, while the slope and offset of the SCT comparison is 1.32 and 2.36 cm/s, respectively. Combining and rearranging the parameterized relationships shows that the SCTs travelled faster than the Microstars for CODAR radial velocities less than -4 cm/s and greater than 18 cm/s. In between these speeds, the Microstars travelled faster by up to 2 cm/s.

For the comparisons to Iona, the slope and offset of the Microstar comparison is 1.52 and 3.70 cm/s, respectively, while the slope and offset of the SCT comparison is 1.31 and 4.27 cm/s, respectively. When the outliers in the Microstar/Iona comparison are removed, the slope is 1.23, and so the difference in measured slopes between the drifter styles is essentially the same as in the Westshore comparisons. Because the difference in the offsets is small, the slope difference indicates that the SCTs travel faster.

The comparisons indicate two important trends when the HF radar are used as a reference. The first is that SCTS travel faster, and the second is that the slopes are consistent between HF radar stations for a particular drifter. The slope of the SCTs regressions are larger than the Microstar regressions, and the degree to which they differ can be quantified with:

$$\frac{V_r^{SCT} - V_r^{Microstar}}{V_r^{Microstar}} = \frac{(a^{SCT} - a^{Microstar}) + V_r^{radar}(b^{SCT} - b^{Microstar})}{a^{Microstar} + b^{Microstar} V_r^{radar}}, \tag{4}$$

which, ignoring the offset terms temporarily by setting them to 0, becomes:

$$\frac{V_r^{SCT} - V_r^{Microstar}}{V_r^{Microstar}} = \frac{b^{SCT}}{b^{Microstar}} - 1 \tag{5}$$

Inserting the regression slopes of $b^{SCT} \approx 1.3$, and $b^{Microstar} \approx 1.2$ (Table 1), into equation 5, reveals that the SCT drifters travel $\approx 8\%$ faster than the Microstar drifters.

The advantage of using the HF radar as a reference is that the drifter speed difference can be quantified even when the drifters were not simultaneously deployed at the same point. As a check on the drifter speed comparison, we can also compare the drifter speeds directly without reference to the HF radar because both drifter types were released simultaneously in tight clusters on a number of occasions during the experiment. A quick analysis of the first four deployments reveals that the SCTs travelled 15% to 50% faster than the Microstar drifters, suggesting that using the HF radar as a basis for comparison probably underestimates the difference.

4.2 RMS error results (i.e., precision)

The RMS difference between the drifter and radar radial velocities ranged from 11.3 to 17.2 cm/s, and are generally higher than what is observed in other systems (summarized in Sec. 1.2).

One reason for the large RMS errors is that the distribution of velocity differences, particularly in the Microstar/Iona and Microstar/Westshore comparisons, contain a relatively large number of outlier values which are inconsistent with a normal distribution for random errors. This was discussed in Section 4.1.2, where it was shown that the outliers significantly influence the slope of a linear regression between the radar and drifter

velocities. These outlier points also skew the distributions and increase the calculated RMS difference.

For example, the Microstar/Iona comparison contains many large positive values greater than 25 cm/s ($V_r^{radar} - V_r^{drifter}$). Many of these points occur in a 12 hour period when a single drifter was caught in the outflow of the Fraser River on an ebb-to-flood tide sequence (i.e., peak outflow), and again when another drifter entered the outflow region late during an ebb tide (Fig. 13c). Removing these drifters from the statistics decreases the RMS difference from 17.2 to 15 cm/s.

The Microstar/Westshore comparison also contains a relatively high proportion of outliers (Fig. 8). In this case, the outliers are negative residuals. Extracting the data for which $V_r^{radar} - V_r^{drifter} < -25$ cm/s reveals that these large errors occur during two periods in the time series. The first period of large deviations occurs during the same deployment as the one discussed earlier that caused the large errors in the Microstar/Iona comparison. In this case, however, the outlier points occurred as the drifter moved southward near the mudflats offshore of the Iona jetty, a few hours before the drifters entered the Fraser River outflow. The second series of outlier points coincides with the same drifters that were caught in the Fraser River outflow, which were shown to be the source of the large outliers in the Microstar/Iona comparison discussed in the previous paragraph. Removing the outliers from the Microstar/Westshore comparison reduces the RMS error from 15.4 cm/s to 14.8 cm/s.

Many of the large deviations observed in both HF radar systems discussed above can be traced back to a single drifter, and therefore one might suspect that the radar measurements are good, and that the drifter trajectory is not reliable (for example, perhaps the drogue did not submerge fully), because both radars independently compare poorly to it. This is not necessarily true because the large errors occur at different times during a drifter trajectory, and the errors are not consistent over the whole path. With this in mind, the error must arise from errors in the HF radar radial velocities. The particular cases described above likely reflect a known problem of direction finding HF radar systems in highly sheared regions (Kirincich, 2017), such as might be expected near the mouth of the Fraser River. In fact, misidentification of the first order line in such regions can potentially lead to bias in the time-averaged currents.

4.2.1 Random errors: oceanographic or instrumental?

Assuming for the moment that the drifters are an error-free measurement (i.e., no GPS position errors, slip, or windage), then the RMS error is governed by uncertainty in the HF radar measurement. The HF radar velocity uncertainty is comprised of both oceanic variability and instrumental error. Ohlmann et al. (2007) used drifter measurements on the California shelf to show that about 5 cm/s of the total radar RMS error budget is due to oceanic variability on scales not resolved by the HF radar (< 1 - 2 km and 1 hour). Assuming that the unresolved oceanic variability in this study is also 5 cm/s, then half or more of the total uncertainty is instrumental in nature given the RMS differences of 11.3 to 17.2 cm/s. Suggestions to reduce this error are summarized in the conclusion (Sec. 4.4).

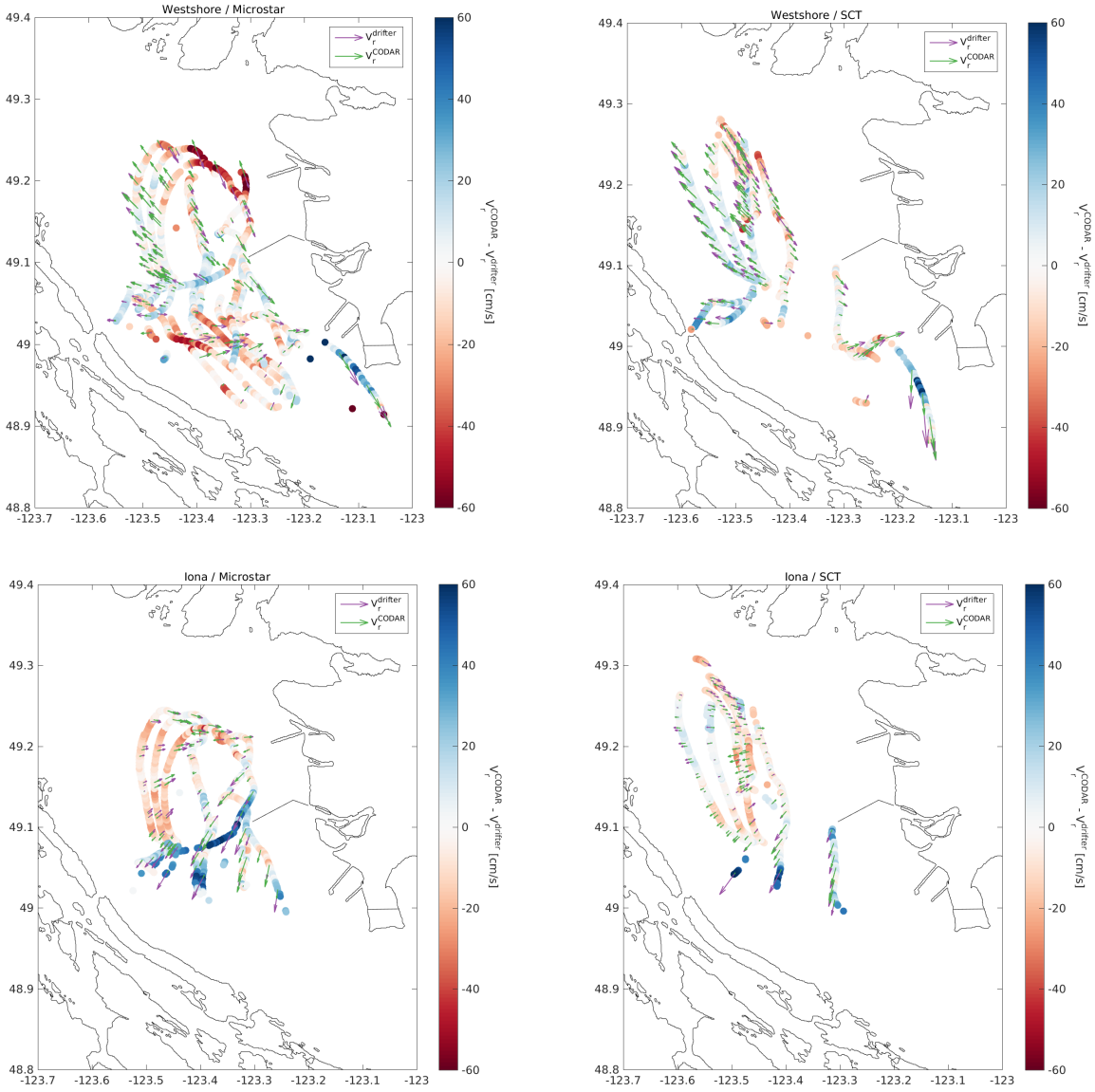

Figure 13: Maps showing the difference between the CODAR radial velocity and the drifter radial velocity for comparison. The colours represent the radial velocity difference, whereas the vectors represent the radial velocities (plotted each hour). In almost all cases the largest errors are due to cases when the drifter velocity was much higher than than the CODAR velocity.

4.2.2 CODAR quality metrics

CODAR computes two statistical metrics, called Temporal and Spatial Quality, to quantify the hourly-averaged radial data uncertainty (CODAR Ocean Sensors, 2013). Both values are computed from the "short-term" radials (≈10 minute), which are the data eventually averaged to form the hourly values. Temporal quality is the standard deviation of the short-term values averaged to form the hourly data. Short-term radials also have an uncertainty that is computed by taking the standard deviation of even shorter time scale measurements. Spatial quality is the average of the standard deviations of the short-term radials. It is named as such because an assumption is made that direction-finding errors dominate oceanographic variability on 10 minute time scales (CODAR Ocean Sensors, 2013).

How do the observed RMS errors compare with the Temporal and Spatial Quality fields provided by CODAR Seasonde software? A cursory look at these metrics for the ONC SoG system reveals that they range from about 5 to 20 cm/s, and are therefore consistent with the RMS errors derived from the drifter/radar comparison.

4.3 Why do the radar and drifters measure different velocities?

Here we discuss some reasons why the HF radar measurements can differ from drifter measurements in terms of oceanographic factors and instrumental factors. In essence, the oceanographic issues are to understand whether Stokes drift contributes to the speed measured by HF radar, and also to understand how instruments with different sampling depths are affected by shear in both the near-surface Eulerian currents and the Stokes drift. HF radar specific instrumental errors are thought to be caused mostly by the processes of first-order line determination and direction-finding.

4.3.1 Stokes drift and Eulerian vertical current shear

Drifters are a Lagrangian measurement whose drift speeds depends on the Eulerian currents and if waves are present, wave-induced Stokes drift. In the case of HF radar, there is no general consensus as to whether the current measurement includes Stokes drift. Furthermore, if HF radar measures Stokes drift, then it is not clear whether it measures one or both of the *full* Stokes drift, which depends on the full wave spectrum, or the *filtered* Stokes drift. The filtered Stokes drift is sometimes considered to be a non-linear correction to the linear gravity wave phase speed originally derived by Barrick and Weber (1977). Mathematically, the expression for the filtered Stokes drift is the same as the expression for the full Stokes drift for waves longer than the Bragg wavelength, but with a modified contribution from shorter waves (e.g., Ardhuin et al., 2009). To further confound the issue, we note that some argue that the theory on which the wave phase correction term of Barrick and Weber (1977) is based is not even valid (Creamer et al., 1989; Janssen, 2009).

Attempts to settle the argument by observations have yielded conflicting results. Observational support that HF radar currents include Stokes drift can be found in Mao and Heron (2008). On the other hand, Röhrs et al. (2015) present observational evidence that HF radar velocity is an Eulerian measurement, but cannot assess whether the

nonlinear phase correction should be made because it is small relative to the statistical measurement uncertainty in their study.

Direct measurements of near-surface shear of the Eulerian currents have been made in the Fraser River estuary (e.g., Tedford et al., 2009) and also near the river mouth (e.g., Crean et al., 1988; MacDonald et al., 2007), but not further out into the Strait. However, we can argue on the basis of water column stratification and measurements in other river plumes that the near-surface flow can be strongly sheared. The drifter/radar comparison was done in a region directly impacted by the large outflow of buoyant water from the river (Halverson and Pawlowicz, 2016), which creates a highly stratified surface layer. A series of CTD profiles from two stations in the study area reveal strong stratification from 1 m to 10 m (Halverson and Pawlowicz, 2011), and while extrapolating CTD measurements to the surface to match the drifter and radar sampling depths is, to some degree, a leap of faith, doing so suggests that it is at least possible for the topmost 1 m to be stratified. Furthermore, significant near-surface shear has been measured in the other highly stratified plumes such as those formed by the Columbia River (Kilcher et al., 2012) and the Connecticut River (O'Donnell, 1998).

Stokes drift is also vertically sheared, but if Stokes drift is important, over what depth scale does it vary? The shear arises because the orbital motion that propagates the wave decays with depth. In a monochromatic wave field, the magnitude of the Stokes drift speed decays exponentially with depth (i.e., $V_S \propto e^{-2kz}$) where k is the wave number for surface gravity waves. If the dominant wave period is 3 s, a typical value measured at the Halibut Bank buoy, then the drift speed is reduced to 63% of the surface value at a depth of $(2k)^{-1} \approx 1.1$ m.

The two drifters in this study and the HF radar all measure different weighted averages of the near-surface shear. The Microstar drifters are most sensitive to the currents at 1 m, but the drogue extends ± 60 cm vertically from the drogue centre (Fig. 2). The SCT total draft is 37.5 cm, although due to their cross sectional profile they weight the upper 7.5 cm more heavily than the lower 30 cm (Fig. 3). In other words, SCTs measure a shallow and thin layer of water, whereas the Microstar drifters measure a thicker but deeper layer of water. In the case of HF radar, Stewart and Joy (1974) showed theoretically that the velocity measurements are an exponentially-weighted average over the uppermost $\lambda_{Bragg}/4\pi$ of the water column, or ≈ 0.5 m at 25 MHz.

The range of vertical dimensions in the measurements is roughly the same as the scales over which shear in the both the Eulerian currents and the Stokes drift can vary. Therefore, we expect that each instrument will report a different speed under identical conditions. For example, in the particular case of a surface-intensified shear flow varying significantly over a vertical scale of 1 m, and in the presence of surface waves, the SCTs would indicate a faster flow than the Microstars. The HF radar would measure a lower velocity than the SCTs, but one cannot say anything about how it would compare to the Microstars without more information about the magnitude of the Stokes drift, and about the degree to which HF radar "feels" Stokes drift.

As mentioned earlier (Sec. 4.1.3), the SCTs travel faster than the Microstars. However, we observe that the average CODAR speeds are lower than the speeds from both drifters, which means that effective sampling depth is not the whole story. One possible explanation is that Stokes drift is a significant component of the drifter velocity, and that

the HF radar only measures the Eulerian velocity. An estimate of the Stokes drift under the sea state conditions commonly observed in this region of the SoG is needed to support this conclusion, which we do not attempt here. To get a feeling for the the magnitude of Stokes drift, we note that in a fetch-limited region, Mao and Heron (2008) find that the Stokes drift speed is about 0.8% of the wind speed (U_{10}), or 4 cm/s for a 5 m/s wind, which, although small, is large enough to be a significant term in the uncertainty budget (Table 1).

4.3.2 First-order line detection

As argued in Sec. 4.2.1, the RMS errors are dominated by instrumental uncertainty. Most of the drifter/radar pair comparisons indicated the potential for some bias, as well. Here we discuss how uncertainty enters the velocity determination, and also why the ONC SoG HF radar cannot reliably measure high flow speeds.

One of the primary sources of instrumental uncertainty is the process of isolating the Doppler bins in the 1st order line from the rest of the spectrum. In order to measure the speed and direction of arrival of the currents, the Seasonde radial processing software must identify the high and low frequency limits of the 1st order line, and then apply the direction-finding algorithm to the Doppler bins in the line.

The algorithm for finding the 1st line requires five user-tuneable parameters. The one we will discuss is the *CurrentVelocityLimit*, which is the maximum expected velocity. Although the 1st region is generally the brightest region of the spectrum and mostly free from spurious energy, in high wave and/or strong current situations, the high-frequency side can be contaminated by power from the 2nd order line. In cases where the 2nd order line blends with the 1st order line, the maximum velocity threshold would effectively cut off the highest frequencies under the assumption that the power contained within them was due to 2nd order scattering.

The maximum current threshold in this experiment was set to 85 cm/s at Westshore and 180 cm/s at Iona. The flow speed can easily exceed 85 cm/s, and sometimes even 180 cm/s, at the mouth of the Fraser River (Cordes et al., 1980). Ideally, the CODAR processing software would leave this region blank if the actual flow speed was greater than 85 cm/s. However, this region is mostly populated with radial velocities, which could be the result of a direction-finding error (the velocity actually originated elsewhere), or, it could be the result of a spatial interpolation from surrounding points (the radial site software interpolates over small azimuthal gaps). Either way, the velocity will be lower than the actual velocity. We hypothesize that this explains the tendency for the outlier points discussed in Section 4.2 to occur near the Fraser River mouth.

4.3.3 Direction-finding errors

The footprint of the SoG CODAR array contains within it areas of land. For example, the Westshore radial footprint covers some of the Gulf Islands, which are located along the western edge of the Strait of Georgia. Although high frequency radio waves propagate over land, the waves are severely attenuated, and echos originating from land are likely to fall under detection limits. Therefore, if a radial velocity is assigned to a location on land,

then it must be the result of a direction-finding error. Values on land are masked during the standard Seasonde processing, but the software was configured to retain and flag such values. Here we use this feature to assess the performance of the direction-finding ability of the Westshore system.

Analysis of CODAR data over land and water is extended by summing all "spatial counts" from the Westshore station over 144 hours (6 days) of observation from 11 to 15 Dec 2014. Plots show that counts over land are 50 to 100% of those over water. This suggests significant errors in data location, since correct placement of CODAR returns would show none over land. Azimuth errors are the likely cause. Range errors should not be a factor, since the electronic gating involved can be extremely efficient.

Counts at a range of 19 km over land are comparable to those over water (Fig. 14). At this range 7 cells are flagged as land. Three are flagged at 18.5 km, and one at 18 km. This last is at an azimuth of 217.5° where the neighbouring cell at 18.5 km is flagged as water and the next cell at 19 km is flagged as land. This seems odd.

CODAR seems to have only a poor ability to detect land, presumably due to inaccurate azimuth determination. Land counts at larger ranges show minima at about 25% of the counts over land, but Fig. 16 and the left side of Fig. 15 show totals grading up to match the values over water. This grading might be explained by a Gaussian azimuth error distribution with a 40° to 60° width at half height, but in that case, the counts at the land/water boundary should be intermediate between counts on land and water far from the boundary. In fact, CODAR web pages suggest that the expected error is due to the direction-finding algorithm breaking down, and presumably returning a random azimuth. This would be consistent with the more sudden rise in counts on the right side of Fig. 15 and with the lack of a measured drop in counts on water, but near land. Perhaps the best error model for CODAR azimuths should be a mixture of random and Gaussian, with random predominating.

The distribution of counts with azimuth shown in Fig. 17 shows more data being detected from due south of the Westshore station. This might be expected since higher currents will tend to occur there, north of Boundary Pass. The relatively narrow width of the peak at 180° suggests a relatively narrow Gaussian error distribution (less than about 20°) in azimuth determinations. This narrow width should also apply to the error model for other azimuth determinations, unless these higher currents are easier to locate.

The errors indicated by Figs. 14 to 16 suggest a serious limit to CODAR's accuracy in locating the currents it measures, and hence in determining surface current fields. Errors might be less in a more uniform current field, but might be significant even then. The nature of the error model is still to be determined.

Range errors should not be a factor, but should be checked. Figures 18 and 19 show the distribution of CODAR returns with range at a time when returns are good. Figures 20 and 21 show distributions when data are missing at long ranges. The same lack of data is seen in both Figs. 20 and 21, suggesting that the data over land are due to azimuth errors.

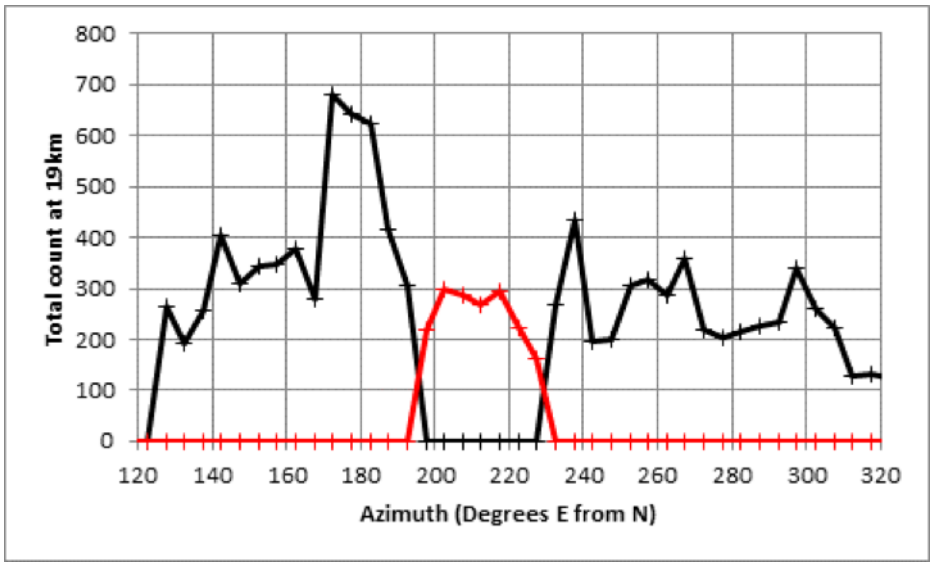

Figure 14: Total counts observed at the Westshore CODAR station from 11 to 15 December 2014 at a range of 19 km. The red line connects counts flagged as being over land.

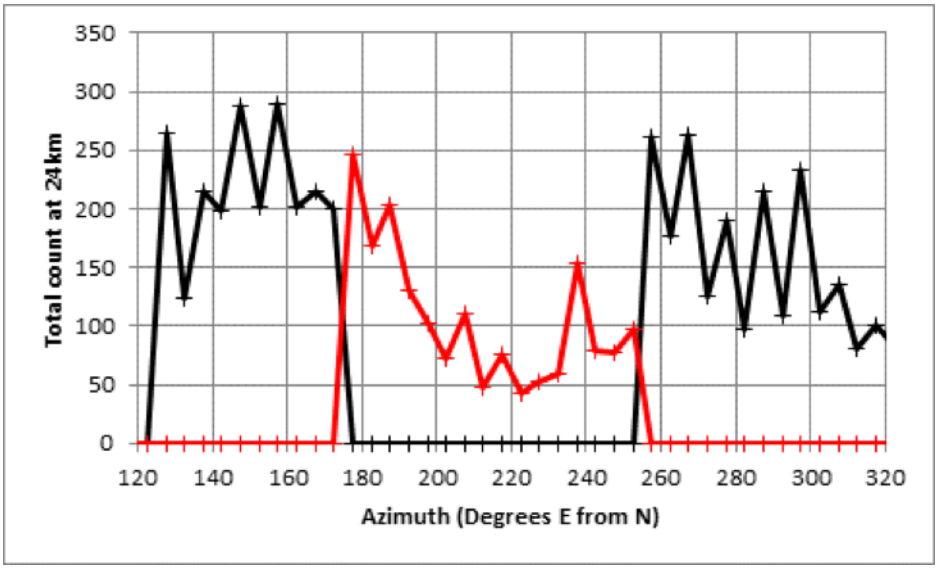

Figure 15: Total counts observed at the Westshore CODAR station from 11 to 15 December 2014 at a range of 24 km. The red line connects counts flagged as being over land.

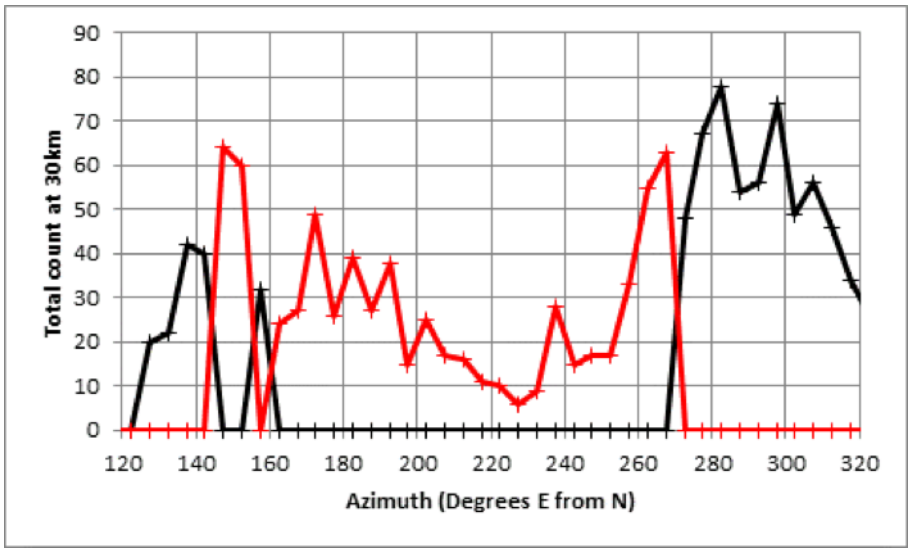

Figure 16: Total counts observed at the Westshore CODAR station from 11 to 15 December 2014 at a range of 30 km. The red line connects counts flagged as being over land.

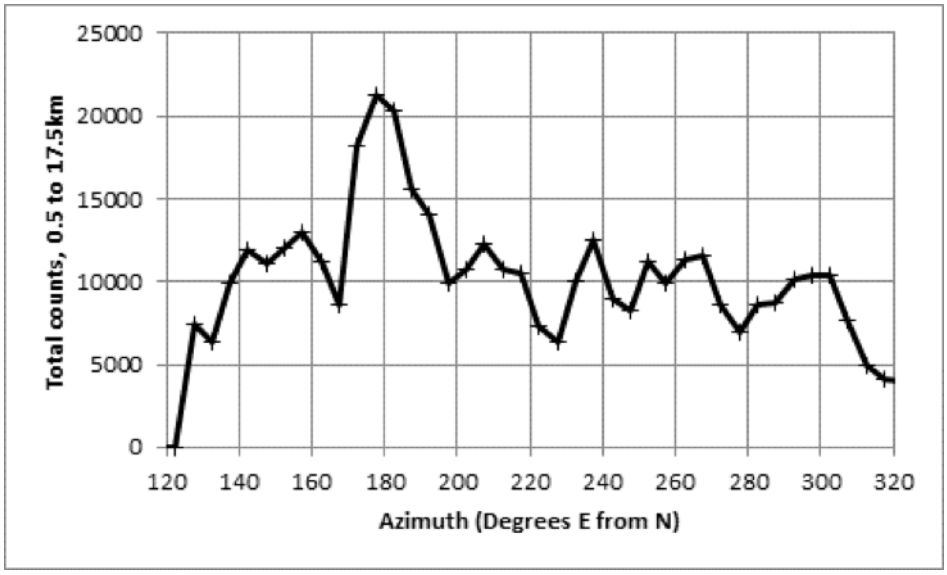

Figure 17: Total counts observed at the Westshore CODAR station from 11 to 15 December 2014 summed for all ranges out to 17.5 km, the first range at which land (Galiano Island) is detected. The distribution shows a peak at 180° whose relatively narrow width suggests that the azimuth error model might have a Gaussian full width to half maximum of less than about 20°. A similar peak is seen in Fig. 14, at a range of 19 km.

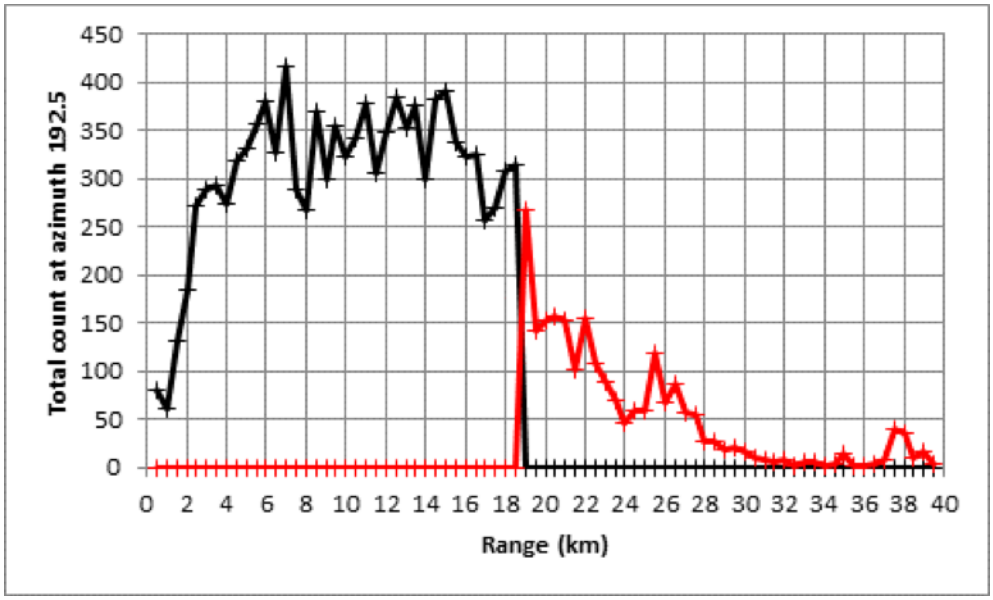

Figure 18: Total counts observed at the Westshore CODAR station from 11 to 15 December 2014 for all ranges at an azimuth of 192.5°. The red line connects counts flagged as being over land. Counts over land could be interpreted as due to poor range gating, but this seems unlikely.

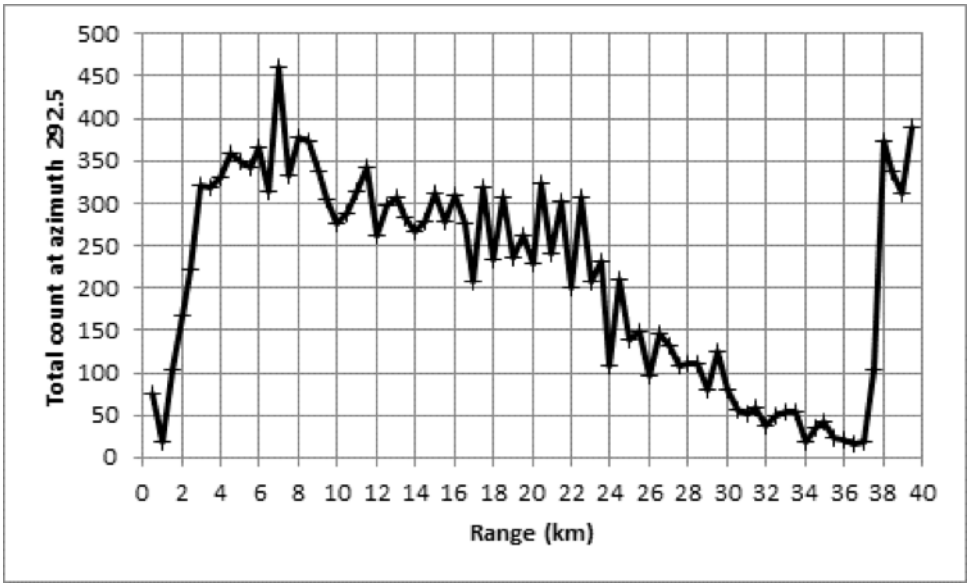

Figure 19: Total counts observed at the Westshore CODAR station from 11 to 15 December 2014 for all ranges at an azimuth of 292.5°. No land is covered at this azimuth. Counts stay roughly constant to arrange of about 23 km, then drop to near zero by 37 km. The return to high values at ranges 38 km and above, needs to be checked.

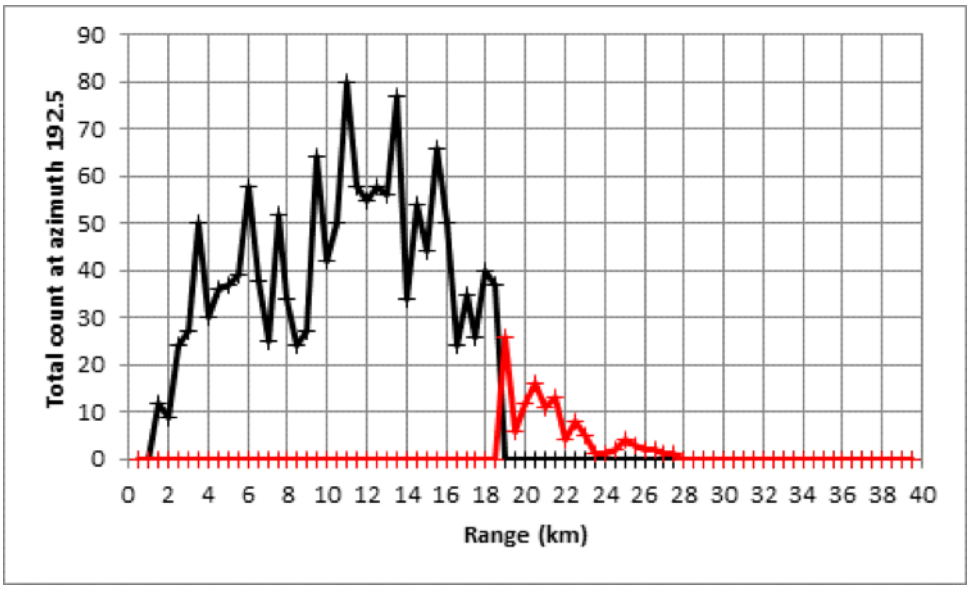

Figure 20: Total counts observed at the Westshore CODAR station for all hours on 13 December 2014 for all ranges at an azimuth of 192.5°. The red line connects counts flagged as being over land. Few data were recorded at long ranges on this day. Counts for 14 and 16 Dec were similar, 15 Dec showed slightly more long range data.

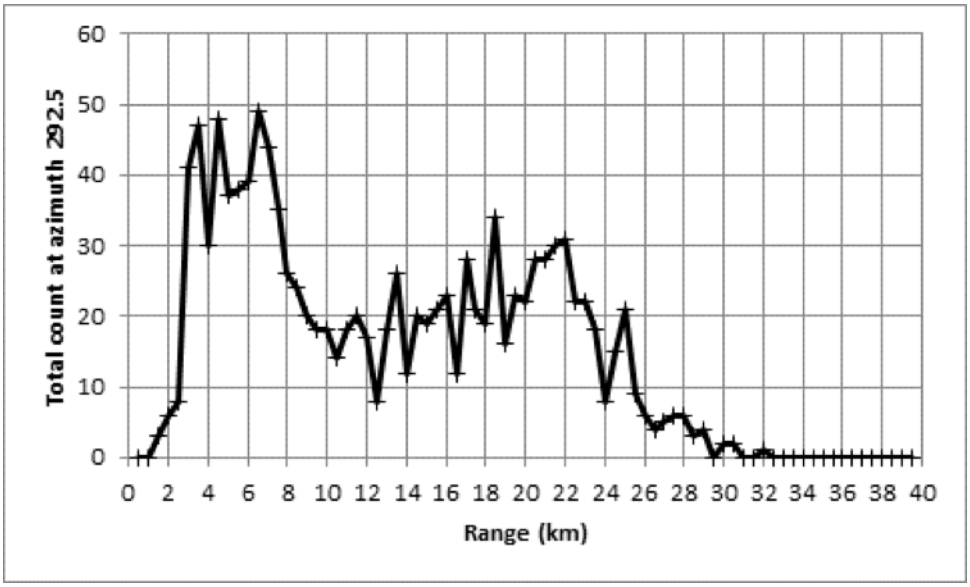

Figure 21: Total counts observed at the Westshore CODAR station for all hours on 13 December 2014 for all ranges at an azimuth of 292.5°. No land is covered at this azimuth. Few data were recorded at long ranges on this day. Counts for 14 and 16 Dec were similar. 15 Dec showed slightly more long range data, with a smaller peak at 39 km range.

4.4 Recommendations to improve HF radar data quality

Before discussing different options to improve the data quality, we note that Ocean Networks Canada has installed two more 25 MHz systems in the study area at Georgina Point (VGPT) and Point Atkinson (VATK), and therefore, as of January 2017, four radial sites are operational. This means that the *total* velocities, which are ultimately the quantities of interest for most oceanographic applications, have likely improved because the spatial density of radial vectors, and therefore the number of independent radial values within a 1 km averaging radius, has increased.

However, the radial velocity precision (as quantified by the RMS error and r^2) could likely be increased. Discussed below are three different approaches, which typically involve a more careful consideration of the cross-spectra before radial velocities are derived, rather than considering the radial or total velocities themselves (e.g., Kim, 2015).

1. Implement the stricter radial metric QA/QC criteria developed by Kirincich et al. (2012). Radial metric files contain detailed information on the received signal and the direction-finding algorithm. Radial metric files are an optional output in version 7 of the SeaSonde Radial Site software, but unfortunately, this functionality will not be included in version 8.

2. Use the first-order line detection method developed by Kirincich (2017) in place of the vendor's algorithm. The algorithm is based on image processing techniques, and was shown to result in more accurate current measurements in regions with complex wave and current conditions, including regions where velocity shear is significant, such as near the mouth of Columbia River.

3. Allow first-order detection settings to vary as a function of range. This might be a useful approach to deal with the complex region near the Fraser River mouth. The SeaSonde processing software currently provides this level of customization.

4. Re-site the Iona radial station. This site sits behind a region of extensive mudflats that enhance ground-wave energy loss, therefore reducing the signal-to-noise ratio and reducing the working range.

Acknowledgements

This work was supported by funding from MEOPAR. This study used data collected by Ocean Networks Canada, and distributed by the Ocean Networks Canada Data Archive, http://www.oceannetworks.ca, Oceans Networks Canada, University of Victoria, Canada. The data were downloaded at various times from June 2014 onward, and we worked closely with Ocean Networks Canada staff scientists and data specialist to ensure we were provided with the most up-to-date and highest quality data available. In particular we wish to thank Kevin Bartlett and Marlene Jeffries.

References

Ardhuin, F., Marié, L., Rascle, N., Forget, P., Roland, A., 2009. Observation and estimation of Lagrangian, Stokes, and Eulerian currents induced by wind and waves at the sea surface. Journal of Physical Oceanography 39 (11), 2820–2838. URL https://doi.org/10.1175/2009JPO4169.1

Barrick, D. E., 1977. Extraction of wave parameters from measured HF radar sea-echo Doppler spectra. Radio Science 12 (3), 415–424. URL http://dx.doi.org/10.1029/RS012i003p00415

Barrick, D. E., Evans, M. W., Weber, B. L., 1977. Ocean surface currents mapped by radar. Science 198 (4313), 138–144. URL http://www.sciencemag.org/content/198/4313/138.abstract

Barrick, D. E., Lipa, B. J., March 1999. Using antenna patterns to improve the quality of SeaSonde HF radar surface current maps. In: Anderson, S. P., Terray, E. A., White, J. A. R., 3rd, A. J. W. (Eds.), Proceedings of the IEEE Sixth Working Conference on Current Measurement. Oceanic Engineering Society, Institute of Electrical and Electronics Engineers, pp. 5 – 8.

Barrick, D. E., Weber, B. L., 1977. On the nonlinear theory for gravity waves on the ocean's surface. Part II: Interpretation and applications. Journal of Physical Oceanography 7 (1), 11–21. URL https://doi.org/10.1175/1520-0485(1977)007<0011:OTNTFG>2.0.CO;2

CODAR Ocean Sensors, Sep 2013. Seasonde current vector uncertainties: The start of QA/QC. URL http://www.codar.com/images/news/press/CODAR_news_09_2013/CODAR_News_09_2013_4.pdf

Cordes, R., Pond, S., de Lange Boom, B., LeBlond, P., 1980. Estimates of entrainment in the Fraser River plume, British Columbia. Atmos. Ocean 18, 15–26.

Creamer, D. B., Henyey, F., Schult, R., Wright, J., 1989. Improved linear representation of ocean surface waves. Journal of Fluid Mechanics 205, 135–161.

Crean, P., Murty, T., Stronach, J., 1988. Mathematical Modelling of Tides and Estuarine Circulation: The Coastal Seas of Southern British Columbia and Washington State. No. 30 in Lecture Notes on Coastal and Estuarine Studies. Springer-Verlag, New York.

Crombie, D. D., April 1955. Doppler spectrum of sea echo at 13.56 mc./s. Nature 175 (4459), 681–682. URL http://dx.doi.org/10.1038/175681a0

Halverson, M., Pawlowicz, R., 2016. Tide, wind, and river forcing of the surface currents in the Fraser River plume. Atmosphere-Ocean 54 (2), 131–152. URL http://dx.doi.org/10.1080/07055900.2016.1138927

Halverson, M., Pawlowicz, R., Chavanne, C., 2017. Dependence of 25-MHz HF radar working range on near-surface conductivity, sea state, and tides. Journal of Atmospheric and Oceanic Technology 34 (2), 447–462. URL http://dx.doi.org/10.1175/JTECH-D-16-0139.1

Halverson, M. J., Pawlowicz, R., 2008. Estuarine forcing of a river plume by river flow and tides. J. Geophys. Res. 113.

Halverson, M. J., Pawlowicz, R., 2011. Entrainment and flushing time in the Fraser River estuary and plume from a steady salt balance analysis. J. Geophys. Res. 116.

Hasselmann, K., January 1971. Determination of ocean wave spectra from Doppler radio return from the sea surface. Nature 229, 16–17.

Hubbard, M., Barrick, D., Garfield, N., Pettigrew, J., Ohlmann, C., Gough, M., 2013. A new method for estimating high-frequency radar error using data from Central San Francisco Bay. Ocean Science Journal 48 (1), 105–116. URL http://dx.doi.org/10.1007/s12601-013-0009-y

Janssen, P. A. E. M., 2009. On some consequences of the canonical transformation in the Hamiltonian theory of water waves. Journal of Fluid Mechanics 637, 1–44.

Kilcher, L. F., Nash, J. D., Moum, J. N., 2012. The role of turbulence stress divergence in decelerating a river plume. Journal of Geophysical Research: Oceans 117 (C5), n/a–n/a, c05032. URL http://dx.doi.org/10.1029/2011JC007398

Kim, S. Y., 2015. Quality assessment techniques applied to surface radial velocity maps obtained from high-frequency radars. Journal of Atmospheric and Oceanic Technology 32 (10), 1915–1927. URL https://doi.org/10.1175/JTECH-D-14-00207.1

Kirincich, A., 2017. Improved detection of the first-order region for direction-finding HF radars using image processing techniques. Journal of Atmospheric and Oceanic Technology 34 (8), 1679–1691. URL https://doi.org/10.1175/JTECH-D-16-0162.1

Kirincich, A. R., de Paolo, T., Terrill, E., 2012. Improving HF radar estimates of surface currents using signal quality metrics, with application to the MVCO high-resolution radar system. Journal of Atmospheric and Oceanic Technology 29 (9), 1377–1390. URL https://doi.org/10.1175/JTECH-D-11-00160.1

Lipa, B., Whelan, C., Rector, B., Nyden, B., 2009. HF radar bistatic measurement of surface current velocities: Drifter comparisons and radar consistency checks. Remote Sensing 1 (4), 1190–1211. URL http://www.mdpi.com/2072-4292/1/4/1190

MacDonald, D. G., Goodman, L., Hetland, R. D., 2007. Turbulent dissipation in a near-field river plume: A comparison of control volume and microstructure observations with a numerical model. J. Geophys. Res. 112.

Mao, Y., Heron, M. L., 2008. The influence of fetch on the response of surface currents to wind studied by Hf ocean surface radar. Journal of Physical Oceanography 38 (5), 1107–1121. URL https://doi.org/10.1175/2007JPO3709.1

O'Donnell, J., 1998. Convergence and downwelling at a river plume front. J. Phys. Oceanogr. 28, 1481–1495.

Ohlmann, C., White, P., Washburn, L., Emery, B., Terrill, E., Otero, M., 2007. Interpretation of coastal HF radar-derived surface currents with high-resolution drifter data. J. Atmos. Oceanic Technol. 24, 666 – 680.

Ohlmann, J. C., White, P. F., Sybrandy, A. L., Niiler, P. P., 2005. GPS-Cellular drifter technology for coastal ocean observing systems. Journal of Atmospheric and Oceanic Technology 22 (9), 1381–1388. URL http://dx.doi.org/10.1175/JTECH1786.1

Paduan, J., Kim, K. C., Cook, M., Chavez, F., Oct 2006. Calibration and validation of direction-finding high-frequency radar ocean surface current observations. Oceanic Engineering, IEEE Journal of 31 (4), 862–875.

Pawlowicz, R., Costanzo, R. D., Halverson, M., Devred, E., Johannessen, S., 2017. Advection, surface area, and sediment load of the Fraser River Plume under variable wind and river forcing. Atmosphere-Ocean 55 (4-5), 293–313. URL https://doi.org/10.1080/07055900.2017.1389689

Röhrs, J., Sperrevik, A. K., Christensen, K. H., Broström, G., Breivik, Ø., 2015. Comparison of HF radar measurements with Eulerian and Lagrangian surface currents. Ocean Dynamics 65 (5), 679–690. URL http://dx.doi.org/10.1007/s10236-015-0828-8

Royer, L., Emery, W., 1982. Variations of the Fraser River plume and their relationship to forcing by tide, wind and discharge. Atmos. Ocean 20, 357–372.

Rypina, I., Kirincich, A., Limeburner, R., Udovydchenkov, I., 2014. Eulerian and Lagrangian correspondence of high-frequency radar and surface drifter data: Effects of radar resolution and flow components. J. Atmos. Oceanic Technol. 31, 945–966.

Schmidt, R. O., Mar. 1986. Multiple emitter location and signal parameter estimation. IEEE Transactions on Antennas and Propagation 34, 276–280.

Shearman, E., December 1983. Propagation and scattering in MF/HF groundwave radar. Communications, Radar and Signal Processing, IEE Proceedings F 130 (7), 579–590.

Stewart, R. H., Joy, J. W., 1974. HF radio measurement of surface currents. Deep-Sea Res 21, 1039–1049.

Tedford, E., Carpenter, J. R., Pawlowicz, R., Pieters, R., Lawrence, G., 2009. Observation and analysis of shear instability in the Fraser River estuary. J. Geophys. Res. 114.

A System configuration parameters

Headers from hourly radial files at the Westshore (VCOL) and Iona (VION) to are included to exemplify instrument settings in this study.

A.1 VCOL

%CTF: 1.00
%FileType: LLUV rdls "RadialMap"
%LLUVSpec: 1.18 2012 05 07
%UUID: 8038C88C-E294-4A83-81D4-238F215D3969
%Manufacturer: CODAR Ocean Sensors. SeaSonde
%Site: VCOL ""
%TimeStamp: 2014 09 20 00 00 00
%TimeZone: "UTC" +0.000 0 "UTC"
%TimeCoverage: 75.000 Minutes
%Origin: 49.0180500 -123.1718833
%GreatCircle: "WGS84" 6378137.000 298.257223562997
%GeodVersion: "CGEO" 1.57 2009 03 10
%LLUVTrustData: all %% all lluv xyuv rbvd
%RangeStart: 1
%RangeEnd: 79
%RangeResolutionKMeters: 0.500300
%AntennaBearing: 278.0 True
%ReferenceBearing: 0 True
%AngularResolution: 5 Deg
%SpatialResolution: 5 Deg
%PatternType: Measured
%PatternDate: 2014 07 25 20 47 42
%PatternResolution: 1.0 deg
%PatternSmoothing: 20.0 deg
%PatternUUID: 4F45E6A7-3476-49BE-8F46-FF893191E86B
%TransmitCenterFreqMHz: 24.400000
%DopplerResolutionHzPerBin: 0.001953125
%FirstOrderMethod: 0
%BraggSmoothingPoints: 5
%CurrentVelocityLimit: 85.0
%BraggHasSecondOrder: 1
%RadialBraggPeakDropOff: 501.190
%RadialBraggPeakNull: 79.430
%RadialBraggNoiseThreshold: 4.000
%PatternAmplitudeCorrections: 2.8568 0.6806
%PatternPhaseCorrections: -145.10 -140.40
%PatternAmplitudeCalculations: 1.5527 0.6844
%PatternPhaseCalculations: -153.00 -141.00

%RadialMusicParameters: 40.000 20.000 2.000
%MergedCount: 7
%RadialMinimumMergePoints: 2
%FirstOrderCalc: 1
%MergeMethod: 1 MedianVectors
%PatternMethod: 1 PatternVectors
%TransmitSweepRateHz: 4.000000
%TransmitBandwidthKHz: -299.616272
%SpectraRangeCells: 79
%SpectraDopplerCells: 2048
%TableType: LLUV RDL9
%TableColumns: 18
%TableColumnTypes: LOND LATD VELU VELV VFLG ESPC ETMP MAXV MINV ERSC ERTC XDS
%TableRows: 2151
%TableStart:
%% Longitude Latitude U comp V comp VectorFlag Spatial Temporal Velocity Velocity Spati
%% (deg) (deg) (cm/s) (cm/s) (GridCode) Quality Quality Maximum Minimum Count

A.2 VION

%CTF: 1.00
%FileType: LLUV rdls "RadialMap"
%LLUVSpec: 1.18 2012 05 07
%UUID: D0548053-5445-401F-8032-5C0EED332A33
%Manufacturer: CODAR Ocean Sensors. SeaSonde
%Site: VION ""
%TimeStamp: 2014 09 20 00 00 00
%TimeZone: "UTC" +0.000 0 "GMT"
%TimeCoverage: 75.000 Minutes
%Origin: 49.2158667 -123.2053833
%GreatCircle: "WGS84" 6378137.000 298.257223562997
%GeodVersion: "CGEO" 1.57 2009 03 10
%LLUVTrustData: all %% all lluv xyuv rbvd
%RangeStart: 3
%RangeEnd: 71
%RangeResolutionKMeters: 0.500300
%AntennaBearing: 312.0 True
%ReferenceBearing: 0 True
%AngularResolution: 5 Deg
%SpatialResolution: 5 Deg
%PatternType: Measured
%PatternDate: 2014 03 13 21 18 05
%PatternResolution: 1.0 deg
%PatternSmoothing: 10.0 deg
%PatternUUID: 54575CEE-42D1-4491-9FCF-9AF5C97EC96D
%TransmitCenterFreqMHz: 25.400000
%DopplerResolutionHzPerBin: 0.001953125
%FirstOrderMethod: 0
%BraggSmoothingPoints: 2
%CurrentVelocityLimit: 180.0
%BraggHasSecondOrder: 1
%RadialBraggPeakDropOff: 50.120
%RadialBraggPeakNull: 100.000
%RadialBraggNoiseThreshold: 4.000
%PatternAmplitudeCorrections: 0.3528 0.9740
%PatternPhaseCorrections: 155.70 107.20
%PatternAmplitudeCalculations: 0.5055 0.7222
%PatternPhaseCalculations: 134.70 89.60
%RadialMusicParameters: 40.000 20.000 2.000
%MergedCount: 7
%RadialMinimumMergePoints: 2
%FirstOrderCalc: 1
%MergeMethod: 1 MedianVectors

%PatternMethod: 1 PatternVectors
%TransmitSweepRateHz: 2.000000
%TransmitBandwidthKHz: -299.616272
%SpectraRangeCells: 79
%SpectraDopplerCells: 1024
%TableType: LLUV RDL9
%TableColumns: 18
%TableColumnTypes: LOND LATD VELU VELV VFLG ESPC ETMP MAXV MINV ERSC ERTC XDS
%TableRows: 1445
%TableStart:
%% Longitude Latitude U comp V comp VectorFlag Spatial Temporal Velocity Velocity Spati
%% (deg) (deg) (cm/s) (cm/s) (GridCode) Quality Quality Maximum Minimum Count